NEUROSCIENCE

Astrocyte-derived CCL5-mediated CCR5$^+$ neutrophil infiltration drives depression pathogenesis

Hang Yao[1]†, Si-Yuan Jiang[1]†, Ying-Ying Jiao[1], Zhi-Yong Zhou[1], Zhu Zhu[1], Cong Wang[1], Ke-Zhong Zhang[2], Teng- Fei Ma[3], Gang Hu[1], Ren-Hong Du[1]*, Ming Lu[1,4]*

Cross-talk between the nervous and immune systems is involved in neurological diseases. However, their potential interplay in depression has yet to be elucidated. Here, using single-cell RNA and neutrophil SMART RNA sequencing, we showed that CCR5$^+$ neutrophils were significantly increased in patients with depression and preferentially migrated to the hippocampus in a mouse model of depression. Infiltrated neutrophils engulf neuronal spines and subsequently promote depressive symptoms in male mice. Furthermore, by genetic or pharmacologic disruption, we identified a chemotactic effect of the astrocyte-derived chemokine CCL5 on mediating the infiltration of CCR5$^+$ neutrophils and behavioral disorders in male depressed mice. Our findings therefore highlight the critical role of neutrophils in depression pathogenesis and astrocytes in mediating the dysregulation of innate immune responses and suggest that inhibition of CCL5/CCR5-mediated neutrophil infiltration represents a potential therapeutic strategy for noninfectious brain diseases such as depression.

INTRODUCTION

Depression is a major cause of disability that affects more than 300 million people worldwide (*1*). It is characterized by glial activation, synaptic deficits, and immune dysfunction (*2*–*4*). Currently, the mechanism underlying depression is still largely unknown. Growing evidence has suggested a critical role for innate immunity in neurological diseases (*5*), including the influence of peripheral neutrophils, which have been shown to play detrimental or protective roles in ischemia (*6*), Alzheimer's disease (*7*), viral encephalitis (*8*), and traumatic brain injury (*9*). However, a comprehensive understanding of the interplay between the central nervous system (CNS) and innate immunity in noninfectious brain diseases such as depression is still lacking.

Inflammation has been reported to be a common feature in patients with depression (*10*, *11*). Psychosocial stressors have been shown to increase peripheral cytokine production, which may contribute to the development of depression (*12*–*14*). Systemic inflammation may lead to an increase in peripheral immune infiltration into the CNS, where these cells can directly interact with CNS-resident cells such as astrocytes, microglia, and neurons (*15*, *16*). In particular, CNS-resident astrocytes have been identified as key producers of important chemokines that induce the migration of peripheral immune cells, including neutrophils (*17*, *18*). Notably, the number of neutrophils is significantly greater in the blood of patients with major depressive disorder (MDD) than in that of healthy controls (HCs) (*19*, *20*), suggesting that innate immunity also participates in the development of depression. Recently, it is reported that circulating myeloid-derived matrix metalloproteinase 8 (MMP8) plays important roles in depression (*21*). However, the interactions between the peripheral immune system and CNS-resident cells under stress conditions are largely unknown. For example, what are the main types of immune cells that migrate into the brain during depression? What is the impact of immune cell brain infiltration on depression? What are the signals that drive immune cell migration to the brain in depression? This study seeks to address these questions.

Here, we performed an unbiased analysis of single-cell RNA and neutrophil SMART RNA sequencing (SMART-seq) data from patients with depression and found that the CCR5$^+$ neutrophil population was significantly increased in patients with depression and that CCR5$^+$ neutrophils migrated preferentially to the hippocampus in a mouse model of depression. In addition, we revealed a previously unidentified chemotactic interaction between astrocyte-derived CCL5 and peripheral CCR5-expressing neutrophils that contributes to the progression of depression. By directly targeting the CCL5-CCR5 chemotactic axis and neutrophil infiltration, our results provide a potential therapeutic approach for treating depression and shed light on the pathological roles of innate immunity in depression.

RESULTS

Single-cell RNA sequencing reveals an increase in the number of neutrophils in depressive patients

To investigate the pathological changes in different immune cell types in depression, we applied single-cell RNA sequencing (scRNA-seq) to blood collected from three patients with MDD and HC. After Louvain clustering of 49,250 cells, canonical markers were used to identify seven major cell types [neutrophils, T and natural killer (NK) cells, B cells, monocytes, plasma cells, basophils, megakaryocytes, and eosinophils] based on uniform manifold approximation and projection (UMAP), which showed high integration quality reflected by the cellular distribution on dimension reduction graphs (Fig. 1, A to C, and fig. S1). We detected an increase in neutrophils in patients with MDD relative to HC (Fig. 1D). To examine the signature profile of neutrophils in MDD patients, we performed Gene Ontology (GO) enrichment and Kyoto Encyclopedia of Genes and Genomes (KEGG) enrichment analyses of biological processes,

[1]Jiangsu Key Laboratory of Neurodegeneration, Department of Pharmacology, Nanjing Medical University, Nanjing 211166, P.R. China. [2]Department of Neurology, The First Affiliated Hospital of Nanjing Medical University, Nanjing, P.R. China. [3]Institute for Stem Cell and Neural Regeneration and Key Laboratory of Cardiovascular & Cerebrovascular Medicine, School of Pharmacy, Nanjing Medical University, Nanjing 211166, P.R. China. [4]Changzhou Second People's Hospital, Changzhou Medical Center, Nanjing Medical University, Changzhou 213000, P.R. China.
*Corresponding author. Email: drh@njmu.edu.cn (R.-H.D.); lum@njmu.edu.cn (M.L.)
†These authors contributed equally to this work.

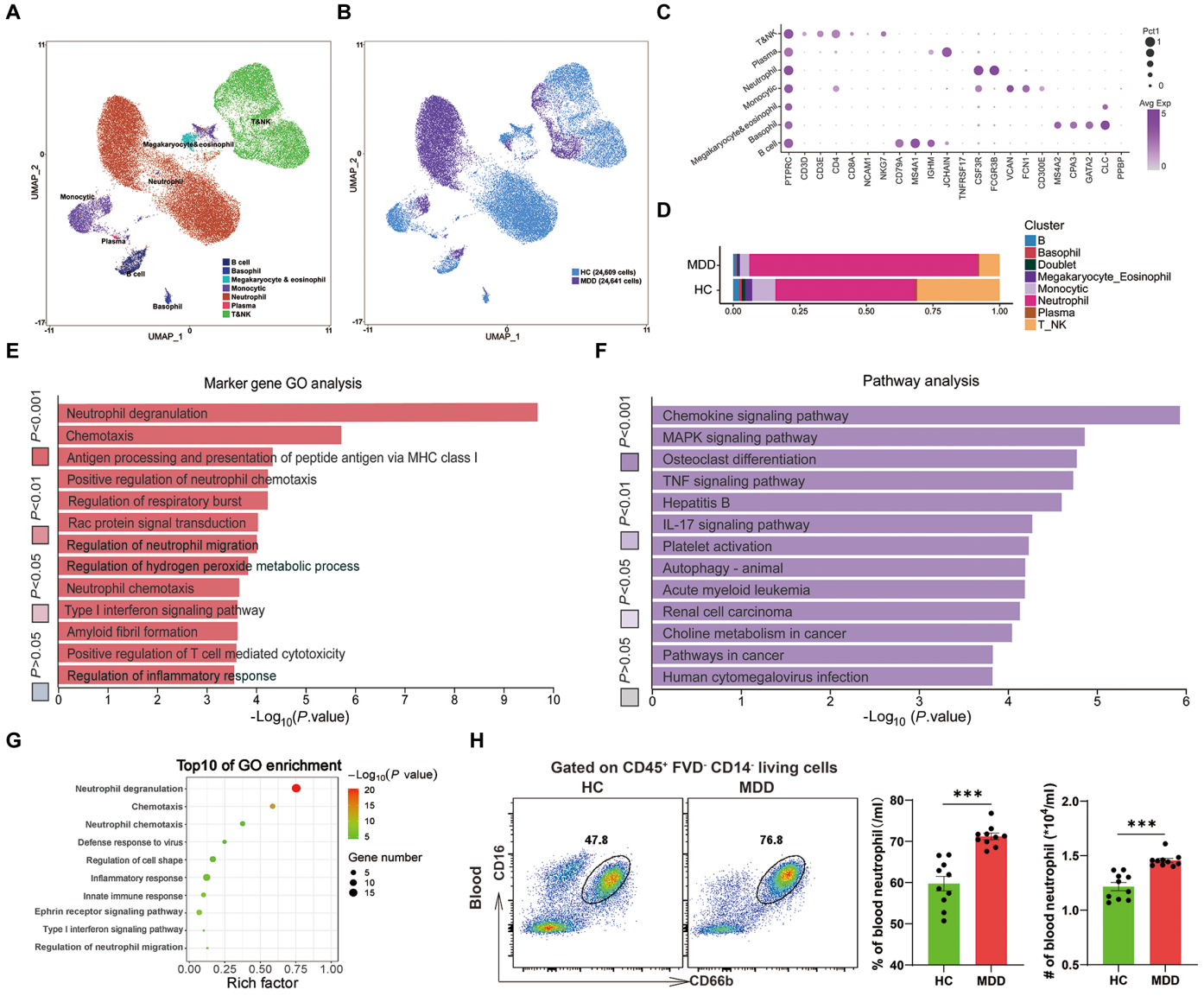

Fig. 1. Single-cell RNA sequencing reveals an increase in the number of neutrophils in depressive patients. (**A**) UMAP embedding plot from three patients with MDD and three HCs showing seven major clusters. (**B**) UMAP embedding plot showing cell distribution of patients (n = 24,641) and HC (n = 24,609). (**C**) Dot plot showing the scaled expression of selected signature genes for each cluster, colored by the average expression of each gene in each cluster scaled across all clusters. (**D**) Proportions of the eight clusters in six samples. (**E**) GO analysis for marker gene of neutrophil clusters. (**F**) KEGG analysis for marker gene of neutrophil clusters. (**G**) GO analysis for DEG of neutrophil clusters between MDD and HC. (**H**) Flow cytometry analysis of neutrophils in blood from patients with MDD and HC (n = 10). The data shown are the mean ± SEM. Student's t test was used. ***$P < 0.001$.

which revealed enrichment of genes associated with neutrophil chemotaxis, migration, degranulation, and innate immune response (Fig. 1, E to G), suggesting that MDD-associated neutrophils are in a state of activation and infiltration. We confirmed a significant increase in neutrophils in patients with MDD compared with HC detected by flow cytometry analysis (Fig. 1H).

To gain insight into the neutrophil characteristics displayed by patients with MDD, we first adopted a chronic social defeat stress (CSDS)–induced murine model of depression (fig. S2, A to D). In line with our findings from patients, flow cytometry analysis revealed increased counts of neutrophils in the blood and spleen of defeated male mice (Fig. 2A and fig. S2E). We further confirmed the enrichment of neutrophils in a chronic unpredictable mild stress (CUMS)–induced murine model of depression. As expected, the number of neutrophils in the blood and spleen of male mice significantly increased after the CUMS procedure (Fig. 2B and fig. S2F). We then performed a principal components analysis (PCA) incorporating SI ratio and the number of neutrophils in blood. The results revealed a obvious separation between control and depressed mice, reinforcing the association between depression and neutrophil dynamics (Fig. 2C). We detected increased numbers of neutrophils, but not T cells or NK cells, in the brain of male mice in both CSDS-induced and CUMS-induced murine models of depression (Fig. 2, D and E, and fig. S3). We also observed distinct patterns

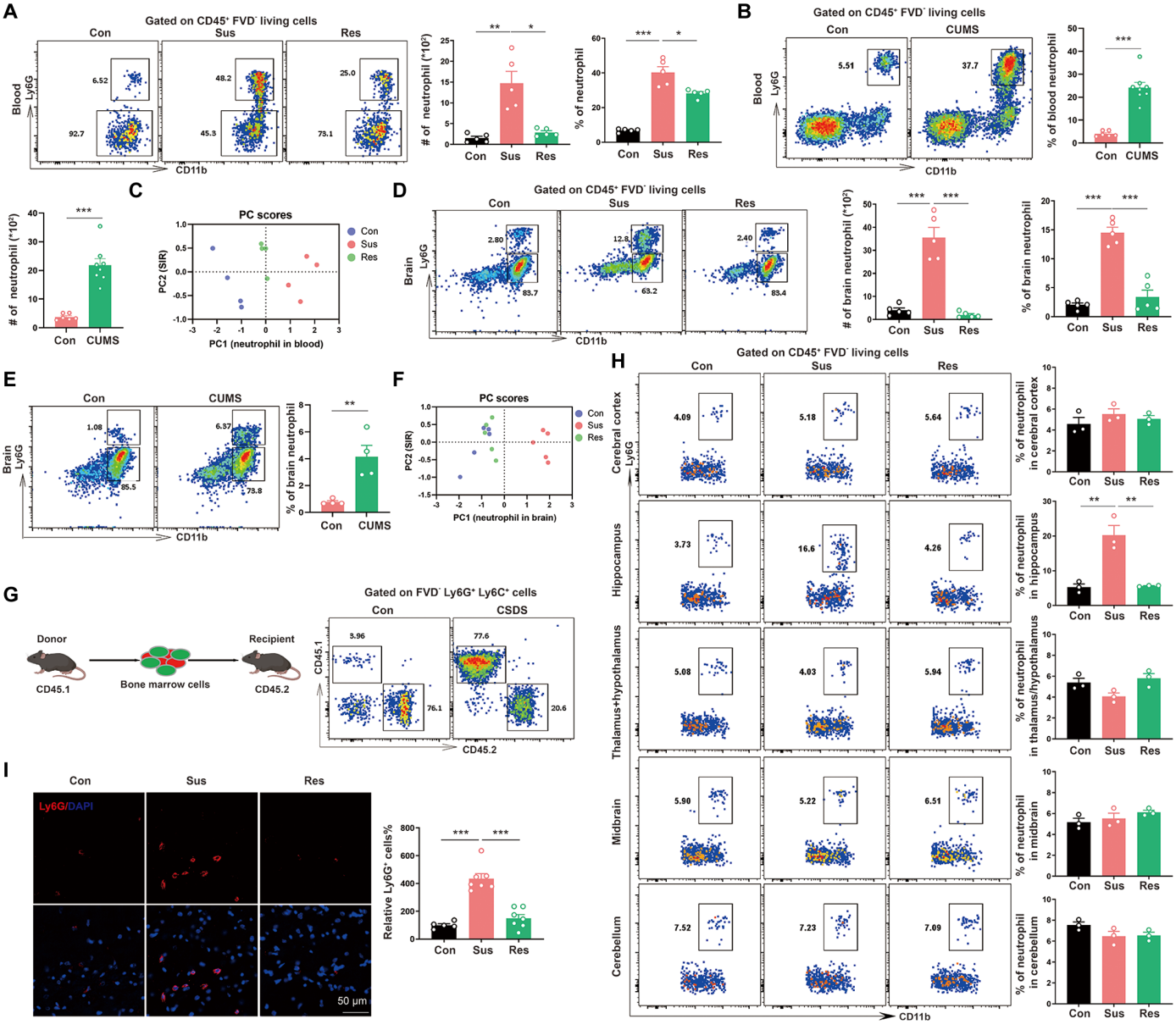

Fig. 2. Neutrophils migrate into the brain in a mouse model of depression. (**A** and **B**) Flow cytometry analysis of neutrophils in blood from mice following CSDS procedure [(A), $n = 5$ animals] and CUMS procedure [(B), $n = 6$ to 8 animals]. (**C**) PCA plot of circulated neutrophil and social interaction ratio (SIR) in control, susceptible mice, and resilient mice. (**D** and **E**) Flow cytometry analysis of neutrophils in brain from mice following CSDS procedure [(D), $n = 5$ animals] and CUMS procedure [(E), $n = 4$ animals]. (**F**) PCA plot of brain neutrophil and SIR in control, susceptible, mice and resilient mice. (**G**) Schematic diagram depicts the tracing of neutrophils. Flow cytometry plots show CD45.1-expressing neutrophils in brain following CSDS procedure. (**H**) Flow cytometry analysis of neutrophils in the cerebral cortex, hippocampus, thalamus/hypothalamus, midbrain, or cerebellum ($n = 4$ to 5 animals mixed). (**I**) Immunofluorescence staining showed the infiltration of neutrophils in hippocampus ($n = 5$ to 7 animals). Con, nonstressed mice; Sus, susceptible mice; Res, resilient mice. The data shown are the mean ± SEM. One-way analysis of variance (ANOVA) with Tukey's post hoc tests was used [(A), (D), (H), and (I)]. Student's *t* test was used [(B) and (E)]. $^{*}P < 0.05$, $^{**}P < 0.01$, $^{***}P < 0.001$.

in the relationship between SI ratio and neutrophil in the brain among control, susceptible mice, and resilient mice (Fig. 2F). These results suggest that circulated neutrophils may infiltrate the brain during depression.

To track the migration of neutrophils to the brain in depression, we performed a bone marrow cotransplantation assay. The recipient CD45.2 mice were irradiated and injected via the tail vein with bone marrow cells from CD45.1 donor mice (fig. S4). After 10 weeks, we assessed the number of cells in the brain. Flow cytometric analysis revealed a significant increase in the number of CD45.1^{+} neutrophils in the brain after the CSDS procedure (Fig. 2G). Next, we examined specific neutrophil-infiltrated brain regions by flow cytometry analysis and found that the number of neutrophils was significantly increased in the hippocampus in male mice, but not in the cerebral cortex, midbrain, thalamus/hypothalamus, or cerebellum (Fig. 2H). Immunostaining and quantification further revealed

that the number of $Ly6G^+$ neutrophils was markedly increased in the hippocampus after the CSDS procedure (Fig. 2I). Blood-brain barrier (BBB) permeability is associated with the infiltration of peripheral immune cells into brain parenchyma after the CSDS procedure (*22*). We therefore tested BBB integrity and found increased BBB permeability and MMP8 levels and reduced claudin-5 expression in the hippocampus of depressed mice (fig. S5). These results indicate that increased numbers of neutrophils migrate into the brain in male mice during depression.

Neutrophil depletion improves CSDS-induced depressive-like behaviors and reduces the engulfment of neuronal synapses

To clarify whether neutrophil infiltration into the brain parenchyma was merely a phenomenon accompanying brain stress or pathological activity during depression, we first started to use a Ly6G neutralizing antibody to deplete peripheral neutrophils in male mice during the CSDS procedure; these mice showed no behavioral deficits (Fig. 3A and fig. S6, A to C). Mice treated with anti-Ly6G showed a 99% reduction in the number of neutrophils in the blood and brain, with no reduction in the number of monocytes or macrophages (Fig. 3B and fig. S7A). Compared with the immunoglobulin G (IgG) isotype control, the Ly6G neutralizing antibody substantially improved depressive-like behaviors in male mice, as indicated by increases in the social interaction (SI) ratio and sucrose preference and decreases in the duration of immobility in the forced swim test (FST) and tail suspension test (TST) (Fig. 3, C to F). To directly further examine the pathological roles of neutrophils in depression, we also used a Ly6G neutralizing antibody to deplete peripheral neutrophils in male mice after the CSDS procedure; these mice already exhibited behavioral deficits (Fig. 3G and fig. S6, D to F). As expected, flow cytometry analysis revealed that the Ly6G neutralizing antibody significantly reduced the number of neutrophils in the blood and brain (Fig. 3H and fig. S7B). A significant increase in the SI time and sucrose preference and a substantial reduction in the duration of immobility in the FST and TST were also observed by Ly6G neutralizing antibody–mediated neutrophil depletion after the CSDS procedure (Fig. 3, I to L).

To further test the role of infiltrated neutrophils in depression, we depleted neutrophils via stereotaxic injection of Ly6G neutralizing antibody into hippocampus or medial prefrontal cortex (mPFC) after the CSDS procedure (Fig. 3M and fig. S8A). We found that deletion of neutrophils in the hippocampus, but not in mPFC, significantly improved depressive-like behaviors in male mice including an increase in the SI ratio and sucrose preference and social preference in social conditioned place preference (sCPP) and preference scores in novel (NV) object recognition test (NORT), and a decrease in the duration of immobility in the FST and TST and latency to feed in the novelty-suppressed feeding test (NSFT) compared with IgG isotype control (Fig. 3, N to T, and fig. S8, B to H). These data demonstrate that infiltrating neutrophils may exert damaging effects on depression.

To elucidate the underlying mechanisms by which neutrophils play a pathological role in depression, we applied high-throughput SMART-seq to brain-infiltrated neutrophils and then performed GO analysis of biological processes, which revealed enrichment of neutrophil activation, phagocytosis, and chemotaxis (Fig. 3U). Activated neutrophils exhibit enhanced phagocytic activity, which is associated with multiple diseases (*23*, *24*). We next studied whether neutrophils engulf neuronal spines in depression. Three-dimensional reconstruction revealed that abundant immunoreactive puncta (red) of PSD95, a marker of postsynaptic components, and Ly6G-labeled neutrophils (green) colocalized in the hippocampus of depressed male mice, indicating that infiltrated neutrophils may engulf neuronal spines in depression (Fig. 3V). In addition, Western blot (WB) analysis revealed that the expression of the postsynaptic protein PSD95 and presynaptic terminal protein synaptophysin (SYP) was markedly reduced in isotype-treated depressed male mice, and this decrease was reversed by Ly6G neutralizing antibody–mediated neutrophil depletion (Fig. 3W). Additionally, increases in PSD95 and SYP expression were also observed after neutrophil depletion, as measured by immunostaining (Fig. 3X). These results suggest that increased engulfing of neuronal synapses by neutrophils contributes to depressive-like behaviors in male mice.

The astrocytic CCL5–neutrophil CCR5 chemokine signal is up-regulated in a mouse model of depression

To examine the signature profile of depression-associated neutrophils, we performed secondary clustering on neutrophils using our scRNA-seq data and identified four neutrophil clusters (mainly G5a, G5b, G5c, and immature neutrophils) based on objective bioinformatics criteria (Fig. 4, A to C), with notably greater fractions of G5a and G5b neutrophil clusters but fewer G5c neutrophil clusters in the blood of MDD patients (Fig. 4D). This disease-associated G5a/G5b neutrophil cluster was characterized by elevated expression of chemokine-related receptors, including CCR5, CXCR1, and CXCR2 (Fig. 4, E to G). To identify necessary chemotactic signals needed to facilitate neutrophil migration into the brain in depression, we also isolated brain-infiltrating neutrophils and then performed high-throughput SMART-seq. According to our analysis of the differentially expressed chemotaxis-related genes, CCR5 was markedly up-regulated in neutrophils from depressed male mice (Fig. 4H), which is consistent with our scRNA-seq findings in MDD patients. Significant up-regulation of CCR5 in neutrophils was confirmed by WB analysis in both CSDS-induced and CUMS-induced mouse models of depression (Fig. 4, I and J, and fig. S9). Similarly, flow cytometry analysis revealed the up-regulation of CCR5 in neutrophils from depressed male mice (Fig. 4, K and L). In addition, an increase in CCR5-expressing neutrophils was also observed in the hippocampus of depressed male mice, as measured by immunostaining (Fig. 4, M to O).

We next examined the production of chemokines during depression to assess potential mediators that might promote the migration of neutrophils. Quantitative polymerase chain reaction (qPCR) analysis of 20 chemokine ligands revealed that the expression of the CCR5 ligand CCL5 was significantly increased in the hippocampus of depressed male mice (Fig. 5, A and B). The up-regulation of CCL5 in the hippocampus was also confirmed by WB analysis (Fig. 5, C and D). We next examined which cell populations were associated with CCL5 production. Elevated CCL5 was mainly expressed by astrocytes but not microglia or neurons in lacunosum moleculare layer (LMol) of depressed male mice, as indicated by coimmunostaining of CCL5 with the astrocyte marker glial fibrillary acidic protein (GFAP), the microglia marker IBA1, or the neuronal marker NeuN (Fig. 5, E and F). Moreover, RNAscope in situ hybridization colabeled with GFAP or IBA1 also revealed elevated CCL5 expression in astrocytes (fig. S10), which was further confirmed by flow cytometry analysis (Fig. 5G). These results suggest that the migration of CCR5-expressing neutrophils to the brain may be mediated by increased expression of the site-specific CCR5 ligand CCL5 by astrocytes.

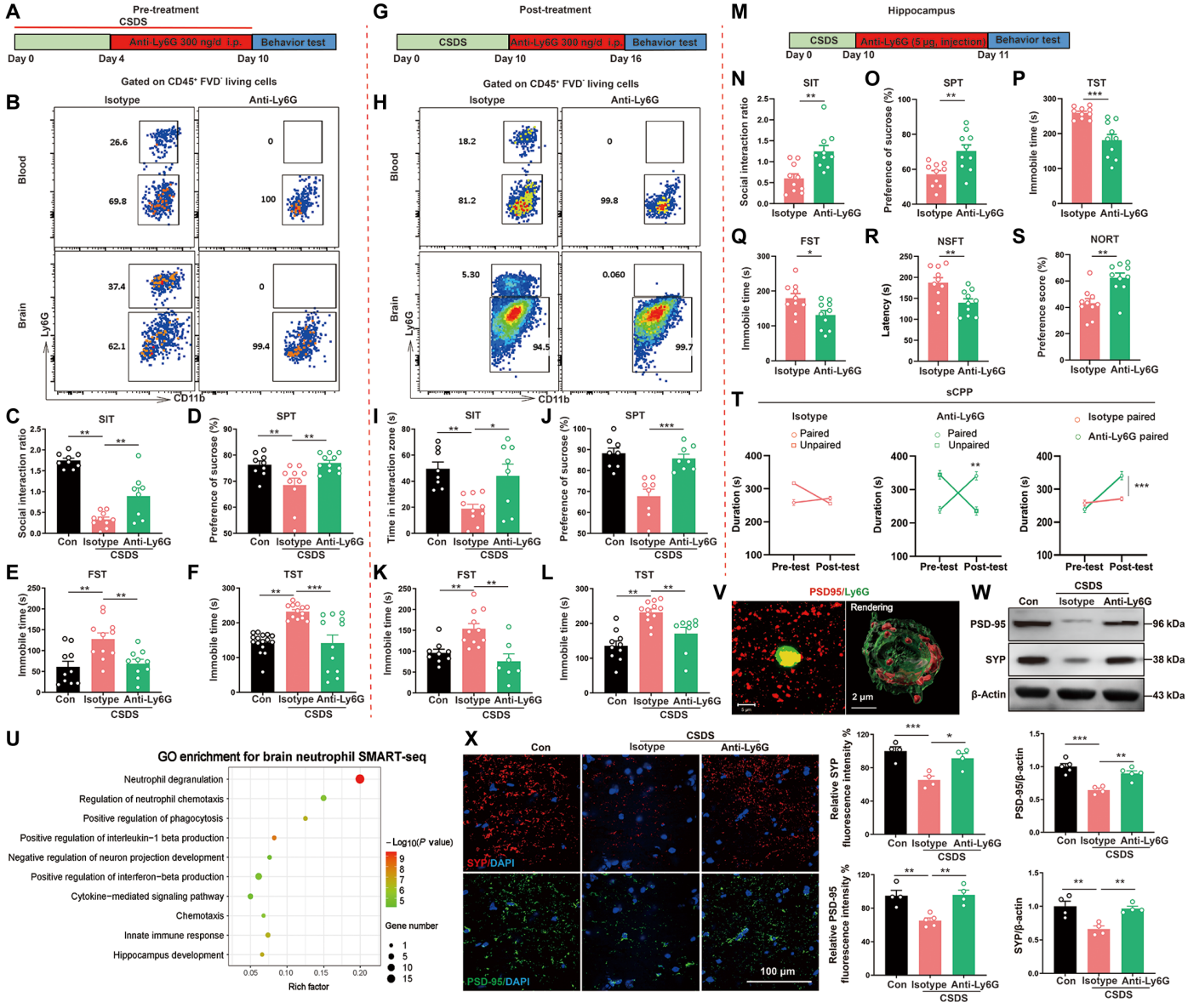

Fig. 3. Neutrophil depletion improves CSDS-induced depressive-like behaviors and reduces the engulfment of neuronal synapses. (**A**) Schematic for Ly6G neutralizing antibody treatment in mice during CSDS procedure. (**B**) Flow cytometry plots show neutrophils in the blood and brain ($n = 5$ animals). (**C**) SI ratio ($n = 8$ to 10 animals). (**D**) Sucrose preference ($n = 9$ to 11 animals). (**E** and **F**) Total immobility time in FST [(E), $n = 10$ to 11 animals] and in TST [(F), $n = 12$ to 16 animals]. (**G**) Schematic for Ly6G neutralizing antibody treatment in mice after CSDS procedure. (**H**) Flow cytometry plots show neutrophils in the blood and brain ($n = 5$ animals). (**I**) Time spent in the interaction zone from SIT ($n = 8$ to 10 animals). (**J**) Sucrose preference ($n = 8$ animals). (**K** and **L**) Total immobility time in FST [(K), $n = 7$ to 11 animals] and in TST [(L), $n = 8$ to 12 animals]. (**M**) Experimental outline. (**N**) SI ratio ($n = 10$ animals). (**O**) Sucrose preference ($n = 10$ animals). (**P** and **Q**) Total immobility time in TST [(P), $n = 10$ animals] and in FST [(O), $n = 10$ animals]. (**R**) Latency in NSFT ($n = 10$ animals). (**S**) Preference score in NORT ($n = 10$ animals). (**T**) sCPP of isotype or anti-Ly6G–injected mice ($n = 10$ animals). (**U**) GO analysis for DEG of brain-infiltrating neutrophil. (**V**) Representative images and three-dimensional (3D) surface rendering of Ly6G$^+$ neutrophils (green) containing PSD95$^+$ puncta (red) in the hippocampus after CSDS procedure. (**W**) WB analysis of PSD95 and SYP expression in the hippocampus ($n = 4$ to 5 animals). (**X**) Representative images and quantitative analyses of immunostaining for PSD95 (green), SYP (red), and DAPI (blue) in the hippocampus ($n = 4$ animals). Isotype, mouse IgG1 isotype control; Anti-Ly6G, Ly6G neutralizing antibody. The data shown are the mean ± SEM. One-way ANOVA followed by Tukey's post hoc test [(C) to (F), (I) to (L), (W), and (X)]. Two-way ANOVA followed by Tukey's post hoc tests (T). Student's *t* test [(N) to (S)]. $^*P < 0.05$, $^{**}P < 0.01$, $^{***}P < 0.001$.

Astrocyte-expressing CCL5 mediates neutrophil brain infiltration and stress susceptibility

To directly determine whether astrocytic CCL5 or microglial CCL5 chemokine signaling is required for neutrophil infiltration and stress susceptibility, we used *Aldh1l1*^{CreER}; *Ccl5*$^{fl/fl}$ mice and *Cx3cr1*^{Cre}; *Ccl5*$^{fl/fl}$ mice in which Ccl5 was conditionally knocked out in astrocytes or microglia but not in other cell types in the brain parenchyma (Fig. 6A). Both *Ccl5* conditional knockout mice and their littermate controls (*Ccl5*$^{fl/fl}$) were subjected to the CSDS procedure. We found a obvious improvement in the depressive-like behaviors of the mice, including an increase in the SI ratio and time spent in the interaction zone and social preference in sCPP and preference scores in

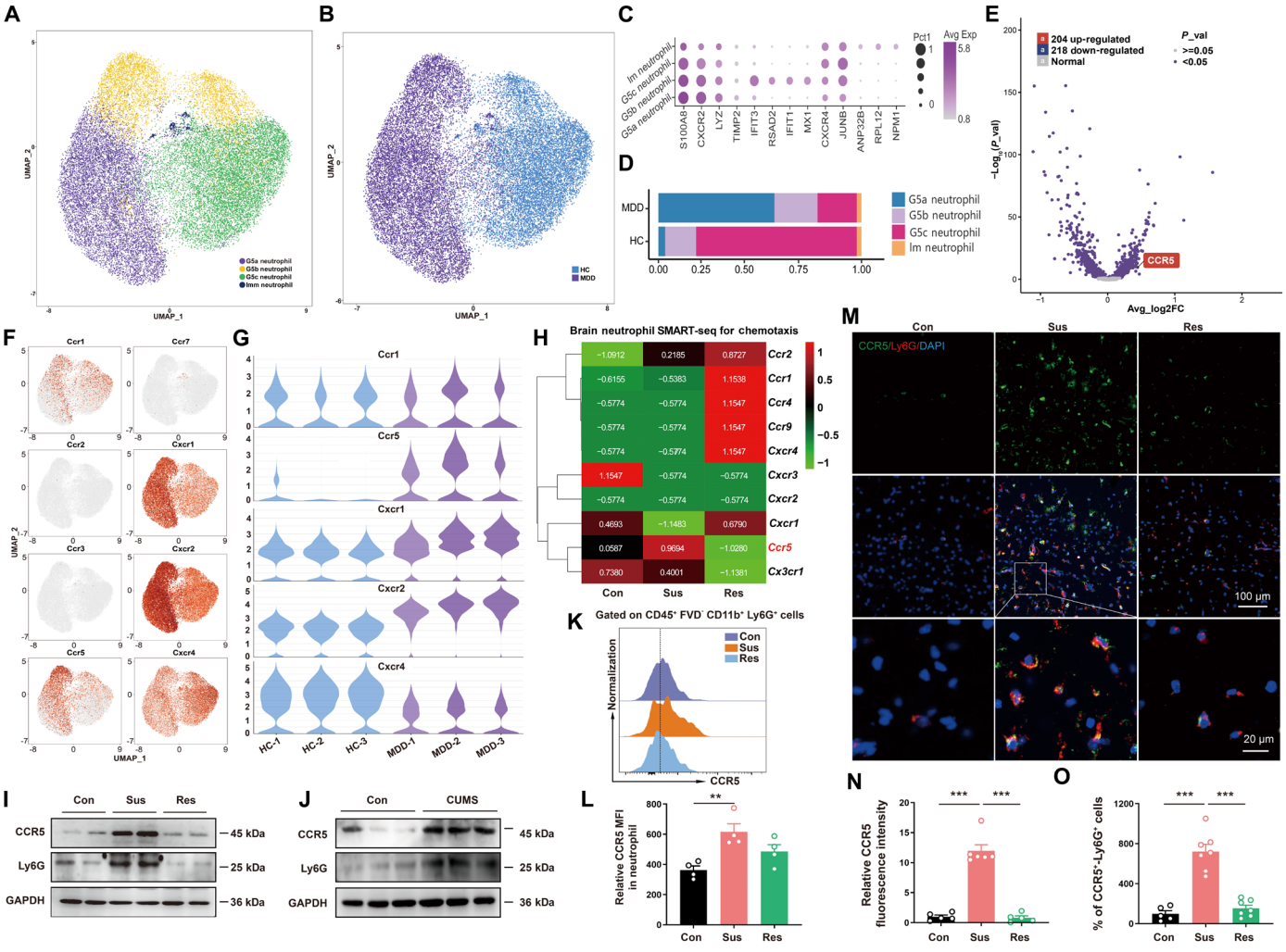

Fig. 4. Neutrophil CCR5 signal is up-regulated in depressive patients and mice. (**A**) Seurat-Recluster analyzed the UMAP embedding plot showing four major neutrophil clusters. (**B**) UMAP embedding plot showing neutrophil distribution of MDD and HC. (**C**) Dot plot showing the scaled expression of selected signature genes for neutrophil cluster. (**D**) Proportions of the four clusters in six samples. (**E**) Volcano plot showing differentially expressed genes in G5a neutrophil cluster between MDD and HC. (**F**) UMAP embedding plot showing the expression of chemokine receptors in neutrophil clusters. (**G**) Violin plots showing the expression of chemokine receptors in neutrophil clusters between MDD and HC. (**H**) Heatmap of the chemokine receptor–related genes determined by SMART-seq of brain neutrophils following CSDS procedure. (**I** and **J**) WB analysis of CCR5 and Ly6G expression in the hippocampus following CSDS and CUMS procedure. (**K** and **L**) Flow cytometry plots and bar graph showing up-regulation of CCR5 in brain neutrophils ($n = 4$ animals). (**M** to **O**) Representative images and quantitative analyses of immunostaining for CCR5 (green), Ly6G (red), and DAPI (blue) in the hippocampus ($n = 5$ to 7 animals). The data shown are the mean ± SEM. One-way ANOVA with Tukey's post hoc tests was used. $^{**}P < 0.01$, $^{***}P < 0.001$.

NORT, and a decrease in the duration of immobility in the FST and TST and latency to feed in the NSFT in the *Aldh1l1*^{CreER}; *Ccl5*$^{fl/fl}$ male mice but not in the *Cx3cr1* ^{Cre}; *Ccl5*$^{fl/fl}$ male mice (Fig. 6, B to J). The infiltration of neutrophils in the brain was also markedly inhibited in the *Aldh1l1*^{CreER}; *Ccl5*$^{fl/fl}$ mice but not in the *Cx3cr1* ^{Cre}; *Ccl5*$^{fl/fl}$ mice (Fig. 6, K to M). These findings demonstrate that astrocyte-expressed CCL5 mediates neutrophil brain infiltration and stress susceptibility.

To further confirm the crucial role of hippocampal astrocytic CCL5 in neutrophil infiltration and stress susceptibility, we stereotaxically injected adeno-associated virus (AAV) carrying GFAP-promoter-sh(*Ccl5*)-EGFP (enhanced green fluorescent protein) into mouse hippocampal regions to specifically down-regulate astrocytic *Ccl5* expression (Fig. 7A and fig. S11). We found that astrocytic *Ccl5* deletion in hippocampus significantly reduced the infiltration of neutrophils in the brain (Fig. 7, B and C), which was accompanied by improvements in depressive-like behaviors after the CSDS procedure (Fig. 7, D to G). However, deletion of *Ccl5* in mPFC or thalamus via stereotaxic injection of CCL5 neutralizing antibody into mPFC or thalamus failed to inhibit the infiltration of neutrophils in the brain and improve depressive-like behaviors in male mice after the CSDS procedure (figs. S12 and S13). Moreover, three-dimensional reconstruction revealed that abundant immunoreactive puncta (red) of PSD95- and Ly6G-labeled neutrophils (green) colocalized in the hippocampus of AAV-vector–injected male mice, and these phenotypes were reversed upon injection of astrocytic AAV-sh(*Ccl5*) (Fig. 7, H and I). Additionally, electron microscopy revealed abundant neutrophils in close proximity to or even enwrapped to the dendritic spines of neurons in the astrocytic AAV-vector–injected male mice, whereas such phagocytic behavior was relatively rare in

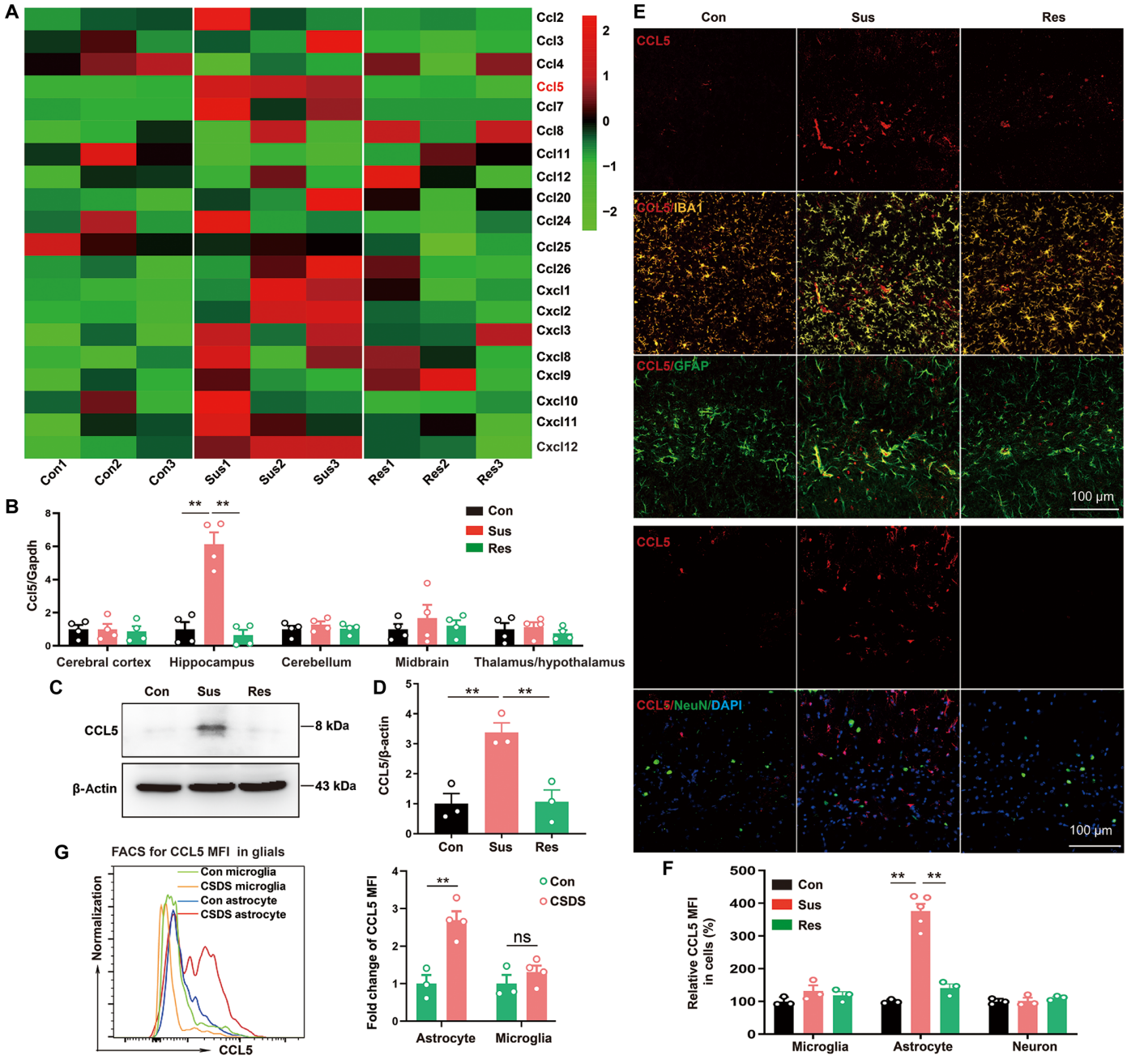

Fig. 5. The chemokine CCL5 is increased in astrocytes in a mouse model of depression. (**A**) Heatmap showing the expression of chemokine ligand in the hippocampus by qPCR analysis. (**B**) qPCR analysis showing the expression of CCL5 in the cerebral cortex, hippocampus, thalamus/hypothalamus, midbrain, or cerebellum ($n = 4$ animals). (**C** and **D**) WB analysis of CCL5 expression in the hippocampus ($n = 3$ animals). (**E**) Representative micrographs of CCL5 (red) costained with IBA1 (orange), GFAP (green), or NeuN (green) in LMol. (**F**) Quantification of CCL5 fluorescence intensity in (E) ($n = 3$ to 5 animals). (**G**) Flow cytometry plots and bar graph showing up-regulation of CCL5 in astrocytes following CSDS procedure ($n = 3$ to 4 animals). The data shown are the mean ± SEM. One-way ANOVA with Tukey's post hoc tests was used [(B), (D), and (F)]. Student's *t* test (G). $^{**}P < 0.01$, $^{***}P < 0.001$.

the astrocytic sh(*Ccl5*)-injected mice after the CSDS procedure (Fig. 7J). Moreover, the displacement of synapses by neutrophils was associated with reduced spine density in control mice but not in astrocytic *Ccl5* deletion mice (Fig. 7, K to N). In addition, WB analysis revealed that the expression of PSD95 and SYP was markedly reduced in control mice after the CSDS procedure but not in astrocytic *Ccl5* deletion mice (Fig. 7, O to Q). To investigate the functional correlates of disturbed synaptic transmission, we performed whole-cell recordings of pyramidal neurons in mouse slices. Individual recordings of pyramidal neurons revealed a significant reduction in the frequency and amplitude of miniature excitatory postsynaptic currents (mEPSCs) in male mice after the CSDS procedure, but this reduction was reversed by the deletion of astrocytic *Ccl5* (Fig. 7, R to T). Compared to that in nonstressed mice, stress induced a significant

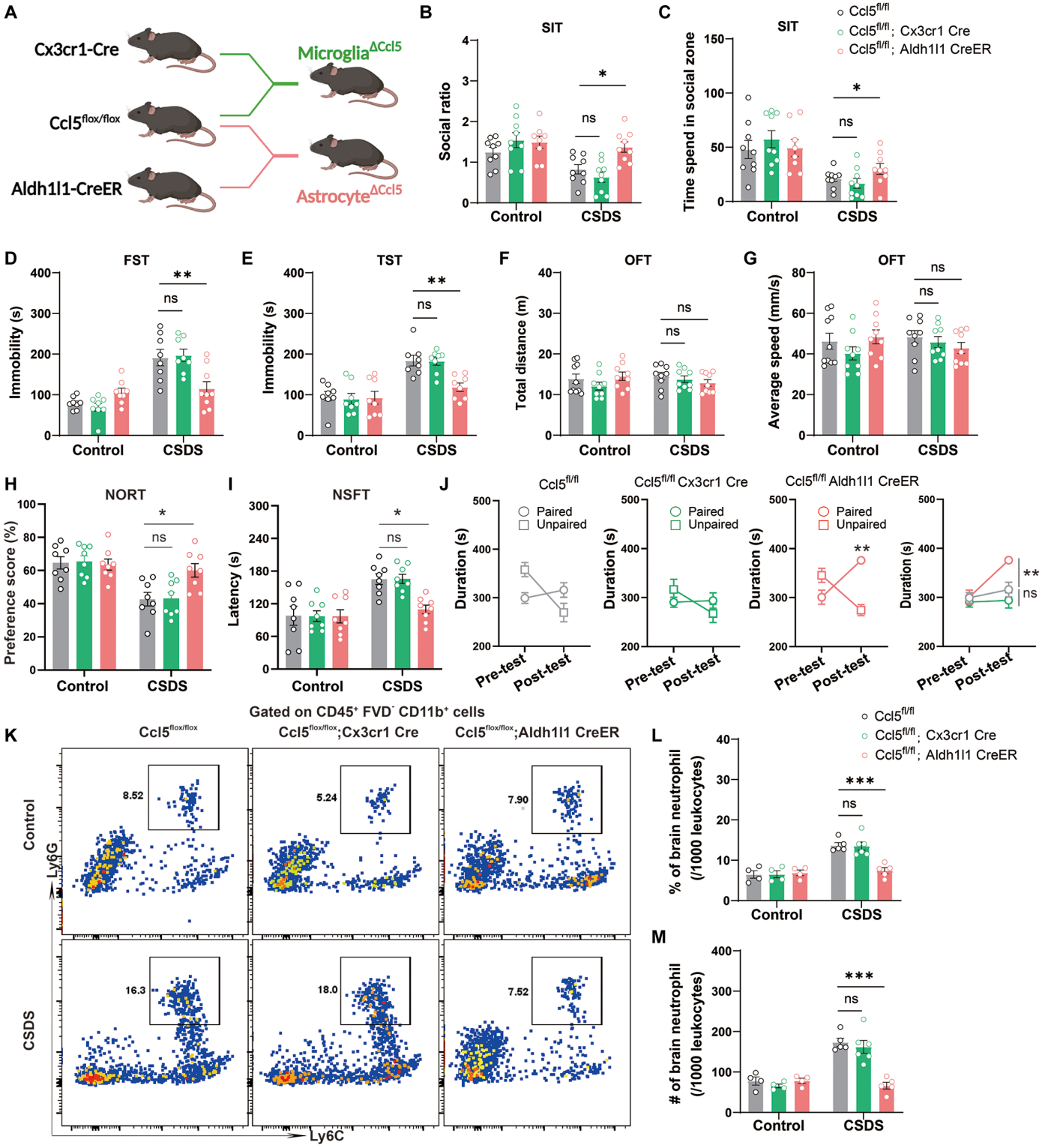

Fig. 6. Astrocytic *Ccl5* deletion prevents neutrophil brain infiltration and stress susceptibility. (**A**) Schematic for astrocytic *Ccl5* deletion or microglial *Ccl5* deletion mice. For Cre-lox experiments, $Ccl5^{fl/fl}$mice were crossbred with $Cx3cr1^{Cre}$ or $Aldh1l1^{CreER}$ mice. (**B** and **C**) SI ratio and time spent in the interaction zone from SIT in $Ccl5^{fl/fl}$ mice, $Aldh1l1^{CreER}$; $Ccl5^{fl/fl}$ mice, or $Cx3cr1^{Cre}$; $Ccl5^{fl/fl}$ mice following CSDS ($n = 9$ animals). (**D** and **E**) Total immobility time in FST ($n = 9$ animals) and in TST ($n = 8$ animals). (**F** and **G**) Movement distance and speed within 5 min was recorded in open field test (OFT) ($n = 9$ animals). (**H**) Preference score in NORT ($n = 8$ animals). (**I**) Latency in NSFT ($n = 8$ animals). (**J**) sCPP of $Ccl5^{fl/fl}$ mice, $Aldh1l1^{CreER}$; $Ccl5^{fl/fl}$ mice, or $Cx3cr1^{Cre}$; $Ccl5^{fl/fl}$ mice ($n = 8$ animals). (**K** to **M**) Flow cytometry analysis of neutrophils in brain from $Ccl5^{fl/fl}$ mice, $Aldh1l1^{CreER}$; $Ccl5^{fl/fl}$ mice, or $Cx3cr1^{Cre}$; $Ccl5^{fl/fl}$ mice following CSDS procedure ($n = 5$ animals). The data shown are the mean ± SEM. Two-way ANOVA with Tukey's post hoc tests was used. $^{*}P < 0.05$, $^{**}P < 0.01$, $^{***}P < 0.001$. ns, not significant.

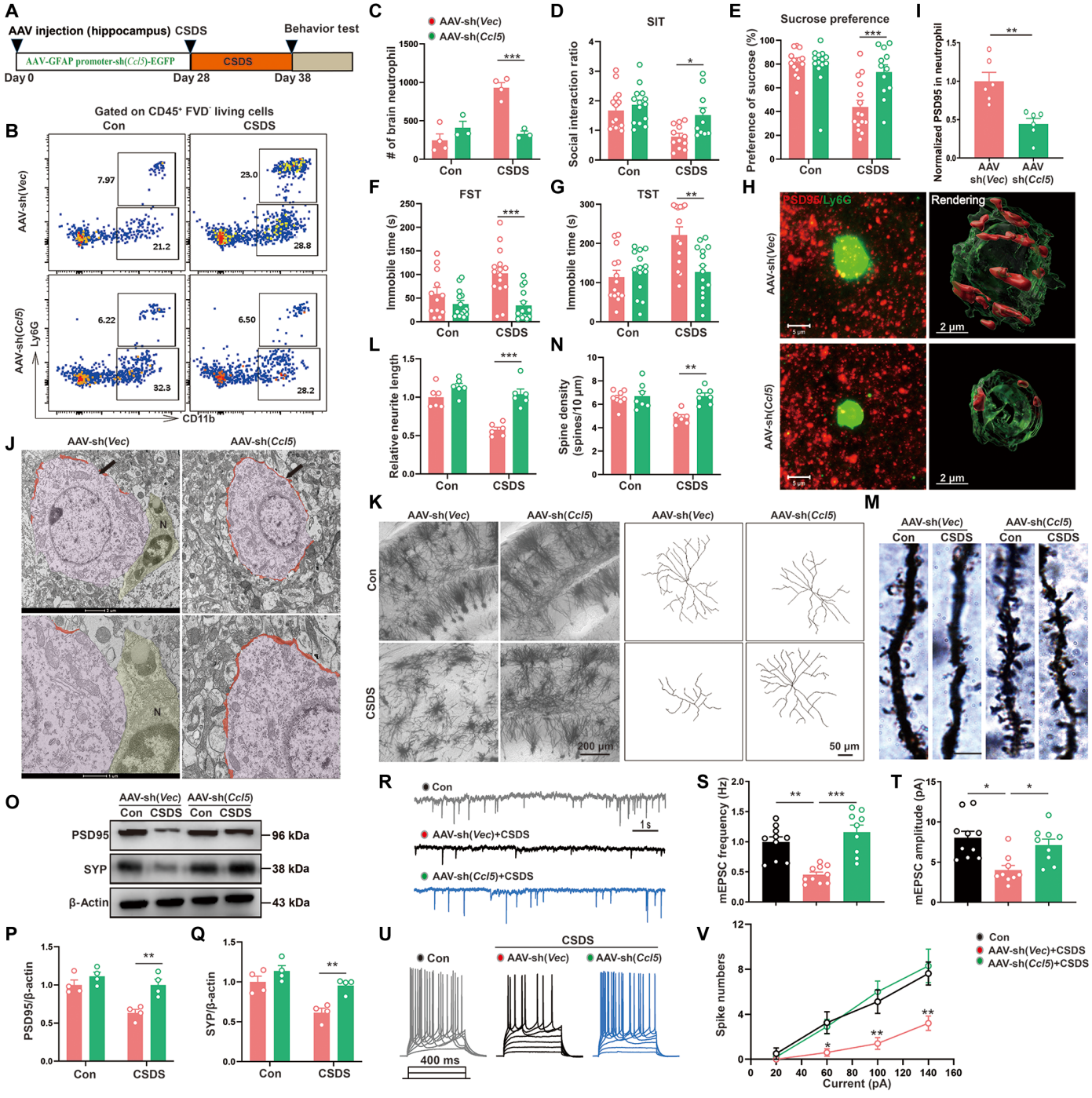

Fig. 7. Astrocyte-expressing CCL5 mediates neutrophil brain infiltration and stress susceptibility. (**A**) Diagram of the experimental design. (**B** and **C**) Flow cytometry analysis of neutrophils in brain from AAV-vector– or AAV-sh(*Ccl5*)–injected mice ($n = 3$ to 4 animals). (**D**) SI ratio ($n = 10$ to 15 animals). (**E**) Sucrose preference ($n = 12$ to 15 animals). (**F** and **G**) Total immobility time in FST [(F), $n = 12$ to 15 animals] and in TST [(G), $n = 14$ to 15 animals]. (**H**) Representative images and 3D surface rendering of Ly6G$^+$ neutrophils (green) containing PSD95$^+$ puncta (red) in the hippocampus after CSDS procedure ($n = 6$ animals). (**I**) Quantification of PSD95$^+$ puncta in neutrophils as indicated in (H). (**J**) Electron micrograph showing a region of hippocampus. In AAV-vector–injected mice, a phagocyte [(N), neutrophils] closely apposing part of a neuronal soma in close vicinity can be observed. Red indicates axosomatic synapses. (**K**) Representative images of neuronal dendrites and 3D reconstruction of neuronal dendrites in mice. (**L**) Summarized data for relative neuronal dendrite length ($n = 6$ animals). (**M**) Representative images of neuronal dendrites by Golgi-Cox staining in mice. (**N**) Summarized data for spine numbers per 10 μm ($n = 6$ animals). Scale bar, 5 μm. (**O** to **Q**) WB analysis of PSD95 and SYP expression in the hippocampus ($n = 4$ animals). (**R** to **T**) Representative traces (R) and summarized data of mEPSC frequency (S) and amplitude (T) from hippocampal pyramidal neurons in mice ($n = 5$ animals). (**U** and **V**) Representative traces (U) and statistical data of step current injection–induced spike numbers (V) from hippocampal pyramidal neurons in mice ($n = 5$ animals). The data shown are the mean ± SEM. One way [(S), (T), and (V)] or two-way ANOVA [(C) to (G), (L), (N), (P), and (Q)] with Tukey's post hoc tests was used. Student's *t* test was used (I). $^*P < 0.05$, $^{**}P < 0.01$, $^{***}P < 0.001$.

decrease in intrinsic membrane excitability in AAV-control–injected mice, while knockdown of astrocytic *Ccl5* expression significantly prevented this stress-induced decrease observed in pyramidal neurons (Fig. 7, U and V). These results indicate that astrocyte-derived CCL5 drives the brain infiltration of neutrophils, which engulf neuronal spines and impair synaptic transmission, leading to depressive-like behavior in male mice.

Inhibition of neutrophil CCR5 alleviates brain neutrophil infiltration and depressive-like behavior in male mice

To evaluate the role of neutrophil CCR5 signaling in neutrophil migration to the brain and stress susceptibility, we used bone marrow chimeric mice harboring *Ccr5*$^{-/-}$ or *Ccr5*$^{+/+}$ bone marrow cells. Lethally irradiated wild-type recipients received bone marrow injections of either *Ccr5*$^{-/-}$ or *Ccr5*$^{+/+}$ bone marrow cells and were then subjected to the CSDS procedure (Fig. 8A). Flow cytometry analysis revealed that the number of neutrophils in the brain was significantly lower (by 70%) in male mice receiving donor *Ccr5*$^{-/-}$ bone marrow cells than in male mice receiving *Ccr5*$^{+/+}$ bone marrow cells (Fig. 8, B and C). As expected, mice receiving donor *Ccr5*$^{-/-}$ bone marrow cells displayed attenuated behavioral deficits, including an increase in the SI ratio, time spent in the interaction zone, and sucrose preference and a decrease in the duration of immobility in the FST and TST, relative to those of recipient mice receiving donor *Ccr5*$^{+/+}$ bone marrow cells (Fig. 8, D to H). Furthermore, Golgi-Cox staining of fixed brain tissues revealed that spine density was markedly increased, and this increase was accompanied by decreased engulfment of synapses in mice receiving donor *Ccr5*$^{-/-}$ bone marrow cells compared to that in mice receiving *Ccr5*$^{+/+}$ bone marrow cells (Fig. 8, I to N). Whole-cell patch-clamp recordings of pyramidal neurons revealed that neuronal activity was significantly enhanced, and this enhancement was accompanied by increased mEPSC amplitude in mice receiving donor *Ccr5*$^{-/-}$ bone marrow cells compared with that in mice receiving donor *Ccr5*$^{+/+}$ bone marrow cells (Fig. 8, O to S). Together, these results imply that inhibition of neutrophil CCR5 alleviates depressive-like behavior by preventing neutrophil-mediated engulfment of neuronal spines.

Enhanced CCR5-expressing neutrophils in patients with depression

To further determine the crucial role of CCR5-expressing neutrophils in the diagnosis and treatment of depression, we examined clinical blood specimens from MDD patients and found that CCR5-expressing neutrophils were significantly increased (Fig. 9, A to C). We next used a mouse model of depression. Similar to our clinical findings, we also observed a sharp increase in CCR5-expressing neutrophils in the blood of CUMS-induced depressed male mice compared with control mice (Fig. 9, D to F). Finally, to investigate whether the pharmacological prevention of CCR5 signaling has therapeutic effects on depression, we intraperitoneally injected male mice with maraviroc, a U.S. Food and Drug Administration–approved CCR5 antagonist, or vehicle (Fig. 9G). A significant reduction in neutrophil brain infiltration was observed in mice treated with maraviroc compared to mice treated with vehicle, which was confirmed by RNAscope in situ hybridization (Fig. 9, H to K). As a result, maraviroc also reversed the behavioral deficits of depressed mice, as indicated by increases in the SI ratio, time spent in the interaction zone, and sucrose preference and decreases in the duration of immobility in the FST and TST (Fig. 9, L to P). However, pharmacological inhibition of CX3CR1 signaling by JMS-17-2 did not reduce neutrophil brain infiltration and improve depressive-like behaviors in male mice after the CSDS procedure (fig. S14). Our data, therefore, indicate that CCR5-positive neutrophils may serve as a potential biomarker and therapeutic target for depression.

DISCUSSION

The exact cell types that link peripheral immune cells and the CNS in depression remain poorly investigated. Our scRNA-seq data revealed a significant increase in the number of neutrophils in patients with depression, which was characterized by elevated expression of chemokines. Consistent with the scRNA-seq findings, we also detected the accumulation of neutrophils in the brain in two mouse models of depression. BBB permeability is involved with the infiltration of peripheral immune cells into brain parenchyma after the CSDS procedure. Our data confirmed increased BBB leakage and MMP8 levels and reduced claudin-5 expression in hippocampus, aligning with Russo laboratory's observations (*22*). Chronic stress may compromise BBB integrity by down-regulating tight junction proteins (e.g., claudin-5) and up-regulating proinflammatory mediators such as MMPs. The resultant BBB hyperpermeability facilitates the transmigration of neutrophils into the brain parenchyma, a process further amplified by stress-induced chemotactic signaling. This strengthens the mechanistic link between chronic stress, BBB disruption, and neutrophil brain infiltration. This elevated neutrophil may be because neutrophils are the first line of defense against invading pathogens, but they are also responsible for tissue destruction during sterile inflammation (*25*). The detrimental effects of neutrophils on the CNS have been recognized in ischemia (*26*) and Alzheimer's disease (*27*). However, whether neutrophils participate in the onset and progression of depression is still unclear. This study revealed the key chemotactic axis that recruits peripheral neutrophils to the brain, which plays an essential role in depression. The number of neutrophils in the blood was consistently correlated with stress susceptibility. Notably, neutrophil depletion at the onset of clinical disease markedly reduced behavioral deficits and neuropathological hallmarks of disease in a mouse model of depression, demonstrating that neutrophils are key players in the development of depression. We also found that the inhibition of neutrophils during the late stages of the disease had a beneficial effect on behavior in depressed animals, demonstrating the therapeutic potential of targeting peripheral neutrophils for the treatment of depression. Although our study was performed in male mice, our scRNA-seq data and clinical blood specimens revealed a significant increase in the number of CCR5-expressing neutrophils from both male and female patients with depression. We assume that the therapeutic potential of targeting neutrophils for the treatment of depression also occurs in female patients.

Immune interactions between the CNS and peripheral organ systems are tightly regulated. Numerous studies on the brain-spleen axis have elucidated the direct regulatory effects of the brain on spleen immune cells (*28*, *29*). Here, a significant increase in the number of neutrophils in spleen was observed in two mouse models of depression. As for the increased neutrophils in the spleen of mouse models, we considered that the CNS directly affect the changes of neutrophils in the spleen by enhancing the spleen control of peripheral sympathetic nerves or induce the granulocyte differentiation of bone marrow hematopoietic stem cells through neuroendocrine

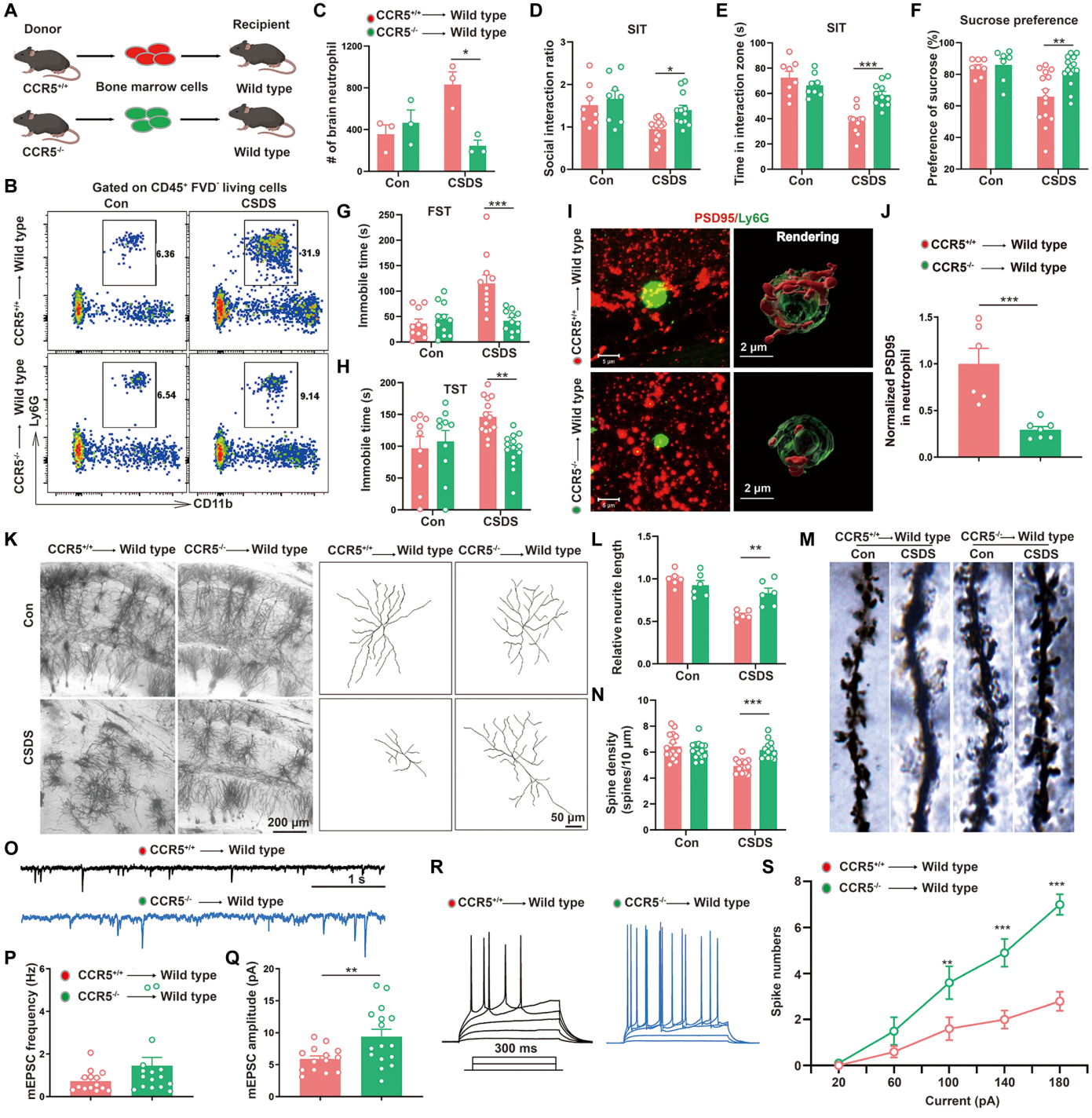

Fig. 8. Inhibition of neutrophil CCR5 alleviates brain neutrophil infiltration and depressive-like behavior in male mice. (**A**) Schematic diagram shows the experimental design. Bone marrow cells were isolated from femur bone marrow of donor *Ccr5*$^{+/+}$ or *Ccr5*$^{-/-}$ mice and then injected into femur bone marrow of recipient mice that were subjected to lethal irradiation. (**B** and **C**) Flow cytometry analysis of neutrophils in brain from *Ccr5*$^{+/+}$ or *Ccr5*$^{-/-}$ bone marrow cell chimeric mice following CSDS ($n = 3$ animals). (**D** and **E**) SI ratio and time spent in the interaction zone from SIT ($n = 8$ to 14 animals). (**F**) Sucrose preference ($n = 7$ to 14 animals). (**G** and **H**) Total immobility time in FST [(G), $n = 10$ to 11 animals] and TST [(H), $n = 9$ to 14 animals]. (**I**) Representative images and 3D surface rendering of Ly6G^{+} neutrophils (green) containing PSD95^{+} puncta (red) in the hippocampus ($n = 6$ to 7 animals). (**J**) Quantification of PSD95^{+} puncta in neutrophils as indicated in (I). (**K**) Representative images of neuronal dendrites and 3D reconstruction of neuronal dendrites in the indicated groups ($n = 6$ animals). (**L**) Summarized data for relative neuronal dendrite length ($n = 6$ animals). (**M** and **N**) Representative images of neuronal dendrites by Golgi-Cox staining and summarized data for spine numbers per 10 μm in *Ccr5*$^{+/+}$ or *Ccr5*$^{-/-}$ bone marrow cell chimeric mice ($n = 6$ animals). Scale bar, 5 μm. (**O** to **Q**) Representative traces (O) and summarized data of mEPSC frequency (P) and amplitude (Q) from hippocampal pyramidal neurons in mice following CSDS ($n = 5$ animals). (**R** and **S**) Representative traces (R) and statistical data of step current injection–induced spike numbers (S) from hippocampal pyramidal neurons in mice following CSDS ($n = 5$ animals). The data shown are the mean ± SEM. Two-way ANOVA with Tukey's post hoc tests was used [(C) to (H), (L), and (N)]. Student's *t* test was used [(J), (P), (Q), and (S)]. *$P < 0.05$, **$P < 0.01$, ***$P < 0.001$.

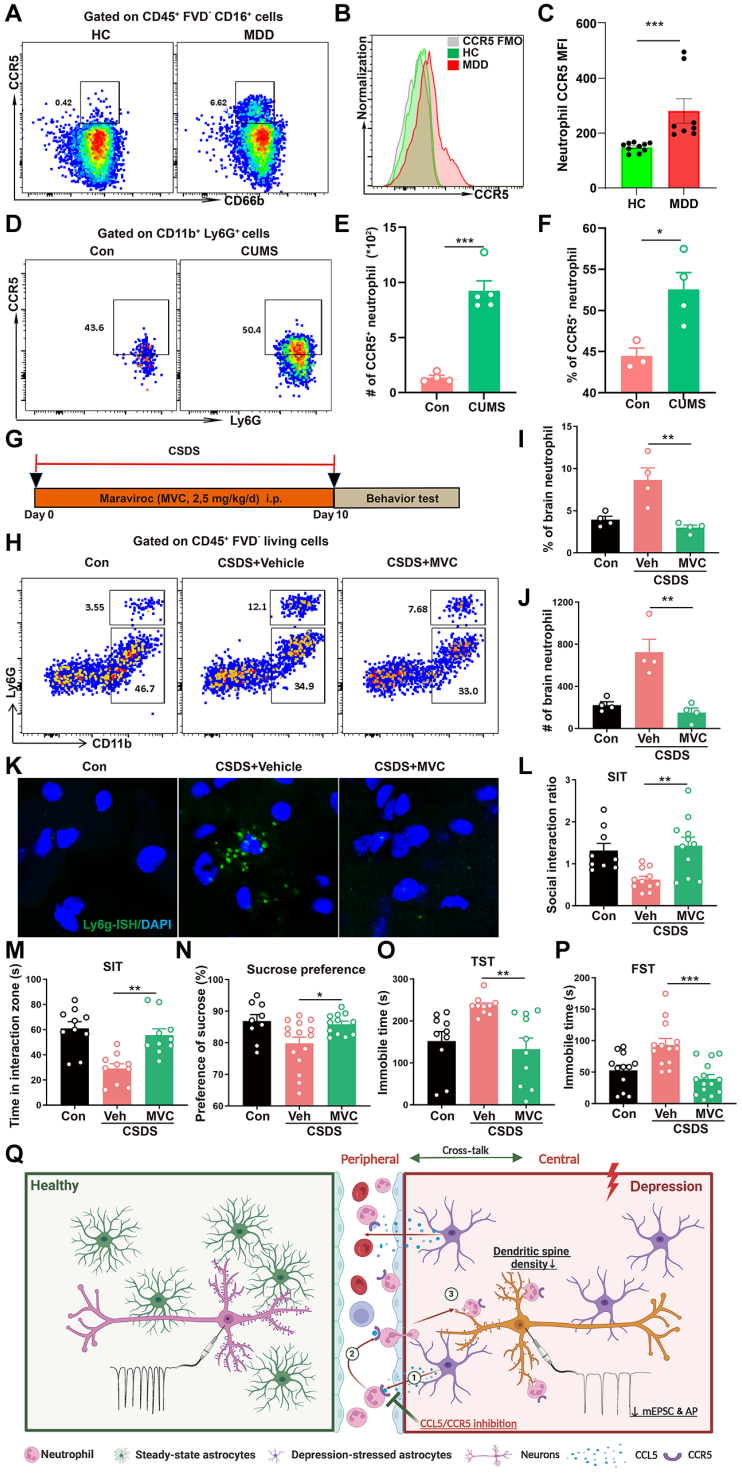

Fig. 9. Enhanced CCR5-expressing neutrophils in patients with depression. (**A** to **C**) Flow cytometry analysis of CCR5-expressing neutrophils in blood from patients with MDD ($n = 8$) or HC ($n = 10$). (**D** to **F**) Flow cytometry analysis of CCR5-expressing neutrophils in blood of mice following CUMS ($n = 3$ to 5 animals). (**G**) Schematic diagram shows the experimental design. (**H** to **J**) Flow cytometry analysis of neutrophils in brain from vehicle- or maraviroc (MVC)–treated mice following CSDS ($n = 4$ animals). (**K**) RNAscope in situ hybridization confirmed reduced neutrophil infiltration in hippocampus of MVC-treated mice. (**L** and **M**) SI ratio and time spent in the interaction zone from SIT in vehicle- or MVC-treated mice following CSDS ($n = 9$ to 11 animals). (**N**) Sucrose preference in the indicated groups following CSDS ($n = 9$ to 15 animals). (**O** and **P**) Total immobility time in FST [(O), $n = 12$ to 14 animals] and in TST [(P), $n = 10$ animals] in the indicated groups following CSDS. (**Q**) Proposed model depicting the crucial role of astrocyte CCL5–neutrophil CCR5 chemotaxis axis in driving neutrophil brain infiltration, consequently contributing to engulfment of neuronal spines and stress susceptibility in depression. The data shown are the mean ± SEM. One-way ANOVA with Tukey's post hoc tests was used [(I), (J), and (L) to (P)]. Student's *t* test was used [(C), (E), and (F)]. $^{*}P < 0.05$, $^{**}P < 0.01$, $^{***}P < 0.001$.

effects and then migrate to the spleen after depressive stress (*30*). The specific regulatory signals of elevated neutrophils in the spleen and their role in depression need to be further studied.

The ability of neutrophils to contribute to brain injury in the CNS has been demonstrated previously, either via the secretion of neutrophil extracellular traps (*31*–*33*) or via production of interleukin-17 (IL-17) (*34*), but the mechanism underlying neutrophil-mediated stress susceptibility has not been determined. Our findings showed that increased neutrophil brain infiltration was associated with reduced numbers of dendritic spines and reduced neuronal excitability in a mouse model of depression. While synaptic elimination is a critical process for normal brain development and plasticity, aberrant synaptic pruning has been implicated in the pathogenesis of various neuropsychiatric disorders. Reduced numbers of dendritic spines and disrupted network connectivity in the hippocampus have been reported both in human patients with MDD (*35*) and in animal stress models (*36*–*38*). Here, we found that stress increased infiltrating neutrophil contacted with dendrites and neutrophil phagocytosis of spines. Infiltrating neutrophils exhibited increased phagocytic activity and promoted excessive engulfment of spines that decrease neuronal activity, resulting in insufficient activation of neurons to cope with stress challenges, which promoted the development of depression-related behaviors. Our studies provide evidence that one potential mechanism underlying stress-induced changes in neuronal activity is excessive phagocytosis of synaptic spines by infiltrated neutrophils in the hippocampus. Moreover, we demonstrated that this process was largely mediated by neutrophil-specific CCR5 signaling and that disruption of neutrophil CCR5 significantly reduced neutrophil phagocytosis of synapses, prevented neuronal excitability changes, and rescued social avoidance behavior in mice.

The exact chemotactic signals that link peripheral immune cells and the CNS remain unclear. CXCL1 has been reported to act as a neutrophil chemoattractant, promoting CXCR2-positive neutrophil migration into the spinal cord gray matter in a mouse model of multiple sclerosis (*39*). A previous study showed that interferon-γ and PDCD1 signaling mediate T cell infiltration and neurodegeneration in tauopathy (*40*). The CXCL10/CXCR3 axis is involved in regulating $CD8^+$ T cell infiltration and neuronal damage in Alzheimer's disease (*41*). Here, we provided evidence that the CCL5-CCR5 axis is required for neutrophils to migrate into the hippocampus in depression. Combined scRNA-seq with SMART-seq analysis of neutrophils revealed increased CCR5 expression in neutrophils, accompanied by the elevated expression of the chemokine CCL5 in astrocytes after stress. Astrocyte-derived CCL5 binds to its receptor CCR5 and leads to the attraction of neutrophils to the hippocampus. Astrocytes make up the majority of the population that induces neutrophil infiltration during depression. Blocking the CCL5-CCR5 chemotactic axis thus prevents the infiltration of neutrophils into stressed brains. Our results provide mechanistic insights into the chemotactic interaction between brain-resident astrocytes and peripheral neutrophils via CCL5. Our study highlights the role of the disease-associated astrocyte-secreted chemokine CCL5 and determine its chemotactic role in recruiting $CCR5^+$ neutrophils into the brain parenchyma and causing subsequent brain injury in depression (Fig. 9Q). Although our study has provided compelling data showing the role of CCL5 in the hippocampus that activates the neutrophil CCR5 in mediating neutrophil brain infiltration and stress susceptibility, we do not exclude the possibility that other types of chemokine signaling or other brain regions may also at play in depression. Several preclinical and clinical studies have linked peripheral immune system alterations to stress-related disorders such as MDD. For example, some types of chemokines, such as CCL2, CCL5, CXCL4, CXCL7, and CXCL8, are increased in depression patients, suggesting that these activated chemokine signals may be involved in the chemotaxis activity of multiple immune cells during depression (*42*, *43*). Furthermore, depressive stress promotes $CCR2^+$ monocyte to infiltrate into the nucleus accumbens and increases MMP8 expression. This increase leads to alterations in extracellular space and neurophysiological changes in the nucleus accumbens, as well as altered social behavior (*21*). Additionally, infiltration of $CCR6^+$ T_H17 cells in hippocampus can induce a depression-like behavior in the mouse model of depression by inhibiting hippocampal neurogenesis (*44*, *45*). These results indicate that complex immune activity, including chemokine signaling specificity and infiltrating immune cell types, exists in various brain regions in depression. Further research is needed to link brain region–specific chemokine signaling and infiltrating immune cell types with specific behavioral changes in depression.

In conclusion, our work demonstrates that CCL5 produced by astrocytes plays a pivotal role in the CCR5-dependent migration of neutrophils into the brain. These recruited neutrophils are likely key drivers of excessive spine engulfment, which is associated with stress susceptibility. Thus, blockade of the CCL5-CCR5 chemokine axis could be a therapeutic approach for depression by inhibiting neutrophil recruitment to the brain.

METHODS

Experimental animals

Ccr5 knockout mice ($Ccr5^{-/-}$) on a C57/B6 background, $Cx3cr1^{Cre}$, and $Aldh1l1^{Cre}$ mice were purchased from the GemPharmatech Laboratory (Nanjing, China). $Ccl5^{fl/fl}$ mice were purchased from Shanghai Model Organisms (Shanghai, China). For Cre-lox experiments, $Ccl5^{fl/fl}$ mice were crossbred with $Cx3cr1^{Cre}$ or $Aldh1l1^{CreER}$ mice. The CD45.1 mice were donated by Y. Shuo (Nanjing Medical University). Mice were bred and maintained in the Animal Resource Centre of the Faculty of Medicine, Nanjing Medical University and had free access to food and water in a room with a 12-hour:12-hour light/dark cycle and an ambient temperature of 20 ± 2°C. All animal procedures were performed in strict accordance with the guideline of the Institutional Animal Care and Use Committee (IACUC-2305014) of Nanjing Medical University.

Human blood samples

Patients with MDD were diagnosed at Jiangsu Province Hospital. Written informed consent was provided by all patients. HCs were identified at the hospital physical examination center. This study was approved by the Medical Ethics Committee of Nanjing Medical University (no. 2024-714) and complied with all relevant ethical regulations. Fresh blood samples were collected from the above populations and stored in heparin anticoagulated tubes. All patients whose peripheral blood is collected for flow cytometry analysis and single-cell sequencing are enrolled according to the following criteria: (i) Patients must be between 30 and 45 years old, regardless of gender. (ii) The patient's weight must be within the normal range (body mass index between 18.5 and 24). (iii) The patients must have been diagnosed with depression for more than 2 years. (iv) Except

for depression, the patient does not suffer from other underlying diseases (hypertension, hyperlipidemia, diabetes, etc.). (v) Except for depression, the patient has not experienced any infectious diseases caused by bacterial or viral invasion in the past 2 months. (vi) The patient has not taken any depression treatment drugs (such as fluoxetine and citalopram) in the past 2 weeks. (vii) The patient has not received any physical therapy for depression in the past 2 months. (viii) Patients with bipolar disorder need to be excluded.

CSDS-induced mouse model of depression

The CSDS paradigm was conducted as previously described (*46*). Adult male CD-1 mice with the age of 20 to 30 weeks old and body weight over 40 g were housed in the defeat cages and used as aggressors in subsequent social defeat experiments. Briefly, mice (male, 8 to 12 weeks) were defeated by a CD-1 aggressor for 10 min daily over 10 consecutive days. The defeated mouse was subjected to continuous psychological stress from a CD-1 mouse through a clear perforated divider, allowing for visual, olfactory, and auditory contact in a shared home cage for the next 24 hours after defeat. Control mice were housed in their home cages and allowed to explore the empty defeat cages for 10 min each day.

CUMS-induced mouse model of depression

Mice (male, 8 to 12 weeks) were individually housed and subjected to 5 weeks of stressors, which were mild and unpredictable in nature, duration, and frequency. Stressors included inversion of day/night light cycle for 24 hours, soiled cage bedding for 12 hours, 45° tilted cage for 18 hours, restraint for 4 hours, food deprivation for 24 hours, water deprivation for 12 hours, cage shaking for 10 min, and tail nip for 1 min (1 cm from the end of the tail). Two different stressors were used in 1 day, and the same stressor was not scheduled in two adjacent days.

Social interaction test

The social interaction test (SIT) was used to determine social avoidance behavior. Briefly, in the first "No target" trial, an empty cage was placed in the interaction zone. In the second "Target" trial, a CD-1 mouse was placed inside the cage in the interaction zone. Each mouse was allowed to freely explore the environment for 5 min with its movement tracked. The mouse was habituated to the chamber in the absence of a CD-1 mouse for 5 min before the test. After each trial, the equipment was cleaned with 75% ethanol to remove olfactory cues. Each trial lasted for 2.5 min, and the duration time in the interaction zone spent by the test mouse was individually measured using Ethovision video tracking software (Noldus Technology). SI ratio was calculated according the following formula: SI ratio = time spent in the interaction zone in the presence of target/time spent in the interaction zone in the absence of target × 100%. Mice with an SI ratio of ≥1 were termed resilient, while mice with an SI ratio of <1 were termed susceptible.

Sucrose preference test

Mice were water deprived for 12 hours and then were allowed to drink from two bottles for 10 hours: One contained 1% sucrose solution, and the other contained only tap water. To prevent the possible effect of side preference in drinking behavior, the positions of the bottles in the cage were switched after the first 5 hours. The consumption of tap water, sucrose solution, and total intake of liquids was estimated simultaneously in the control and experimental groups by weighing the bottles. The preference for sucrose was measured as a percentage of the consumed sucrose solution relative to the total amount of liquid intake.

Tail suspension test

Mouse tails were wrapped with tape from the base to the tip, covering about four-fifths of its length, and fixed upside down on the hook. The immobility time of each mouse was recorded over a 6-min period. Mice were considered immobile only when they hung passively and completely motionless. The duration of immobility of the tail-suspended mice during 6 min was measured with TailSuspScan (Clever Sys Inc., USA).

Forced swim test

Mice were individually forced to swim in an open cylindrical container (diameter, 15 cm; height, 25 cm), containing 14 cm of water at room temperature (about 20 ± 2°C) for 6 min. A mouse was judged to be immobile when it floated in an upright position and made only small movements to keep its head above water. The duration of immobility was recorded during the 6-min testing period by TailSuspScan (Clever Sys Inc., USA).

Novel object recognition test

NORT was conducted in a rectangular open-field arena (50 cm × 30 cm × 20 cm) under dim illumination. Twenty-four hours before testing, mice were habituated to the empty arena for 10 min to reduce exploratory anxiety. During the training phase, two identical objects (objects 1 and 2) were placed in opposite corners of the arena, approximately 10 cm from the walls. Mice were allowed to freely explore the objects for 5 min, with exploration defined as the mouse's nose being within 2 cm of the object while facing it. After a 24-hour retention interval, one familiar object (object 1) was replaced with an NV object (object 2) of similar size but distinct shape and texture. Mice were then reintroduced to the arena for a 5-min test session. Between trials, the arena and objects were thoroughly cleaned with 70% ethanol to eliminate odor cues. Preference score was calculated by dividing time spent with the NV object on the total time spent with both objects × 100. Exploration time for each object was recorded using the TOPSCAN tracking system (Clever Sys Inc., USA).

Novelty-suppressed feeding test

NSFT was conducted in an open-field arena (50 cm × 50 cm × 40 cm) with a single food pellet placed on a white filter paper (10 cm diameter) positioned at the center. Mice were food-restricted for 24 hours before testing, with water available ad libitum. At the start of the test, each mouse was placed in a corner of the arena, and the latency to initiate feeding (defined as the mouse sitting on its haunches and biting the food pellet with forepaws holding the pellet) was recorded for a maximum of 10 min. Immediately following the NSFT, mice were transferred to their home cages containing a preweighed food pellet. The arena was thoroughly cleaned with 70% ethanol between trials to eliminate odor cues. All behavioral recordings were performed using the TOPSCAN tracking system (Clever Sys Inc., USA).

Social conditioned place preference

sCPP was performed as described (*21*). The experiment was conducted after a 1-hour acclimation period in the CPP apparatus. The CPP chamber consists of three distinct compartments: a neutral

central section flanked by two adjacent chambers, each featuring unique wall patterns and floor textures. During pretesting (24 hours before formal testing), mice were permitted to freely explore all three chambers for 15 min, with their time spent in each compartment being recorded. The conditioning protocol involved twice-daily sessions over two consecutive days. Morning sessions paired experimental mice with a juvenile (4 to 5 weeks old) same-sex C57BL/6J mouse in the designated paired chamber for 7 min. Afternoon sessions involved placing mice alone in the nonpaired chamber for an equivalent duration. On test day, mice were again granted unrestricted access to all chambers for 7 min, with time spent in each compartment being automatically quantified using the TOPSCAN tracking system (Clever Sys Inc., USA).

Stereotaxic injection

The surgical procedure was carried out as previously described (*47*). Under anesthesia, 1 μl of AAV [AAV–GFAP promoter–sh(*Ccl5*)–EGFP, 1×10^{13} viral genomes/ml, Gene-Chem, Shanghai, China] was bilaterally delivered into the hippocampus at a rate of 0.2 μl/min using the following coordinates: AP: −1.94 mm; ML: ±1.50 mm; DV: −2.00 mm from bregma. For neutralization of Ly6G in hippocampus or mPFC, 5 μg of anti-Ly6G (BE0075-1, Bio X Cell) was bilaterally injected into hippocampus (AP: −1.94 mm; ML: ±1.50 mm; DV: −2.00 mm) or mPFC (AP: +2.10 mm; ML: 0 mm; DV: −2.50 mm), at a rate of 1 μg/min; for neutralization of CCL5 in thalamus or mPFC, 5 μg of anti-CCL5 (BE0449, Bio X Cell) was bilaterally injected into thalamus (AP: −1.58 mm; ML: 0 mm; DV: −3.50 mm) or mPFC (AP: +2.10 mm; ML: 0 mm; DV: −2.50 mm), at a rate of 1 μg/min. The needle remained in place for 5 min before removal to ensure complete injection of each solution. The skin was sutured, and mice recovered on an electric blanket until fully awake. The entire experiment was performed in a sterile environment.

Immunofluorescence

After perfusion, brain tissue encompassing each hippocampus was cut into 20-μm slices using a freezing microtome (Leica M1950, Nussloch, Germany), as previously described (*48*). Brain slices were incubated with anti-GFAP (MAB360, 1:1000, Millipore, USA), anti-Ly6G (ab25377, 1:400, Abcam), anti-CCR5 (ab7346, 1:500, Abcam), anti-CCL5 (AF478, 1:500, R&D Systems, USA), anti-NeuN (24307S, 1:1000, Cell Signaling Technology, USA), anti-IBA1 (ab5076, 1:1000, Abcam), anti-PSD95 (20665-1-AP, 1:10,000, Proteintech), or anti-SYP (17785-1-AP, 1:10,000, Proteintech) overnight at 4°C and then incubated with Alexa Fluor 555–conjugated antibody (Invitrogen, A21432; 1:1000) or Alexa Fluor 488–conjugated antibody (Invitrogen, A21202; 1:1000) for 1 hour at 20°C. DAPI (4′,6-diamidino-2-phenylindole) (P36931, Life Technologies) visualizes nuclei. Images were acquired by a confocal microscope (Axiovert LSM510, Carl Zeiss Co., Germany) and then processed by ImageJ.

Flow cytometry

Anesthetized mice were perfused with ice-cold phosphate-buffered saline (PBS) as previously described (*49*, *50*). The whole brain tissues were isolated and homogenized on ice. Brain homogenates were digested in Dulbecco's Modified Eagle Medium/F12 containing deoxyribonuclease I (20 U/ml) (Sigma-Aldrich, D5025) and collagenase IV (100 U/ml) (Thermo Fisher Scientific, 17104019), shaking at 250 rpm for 1 hour, and then washed and filtered through a 70-μm cell strainer. The monocytes were isolated by a discontinuous Percoll gradient. Purified cells were incubated with mixed antibodies for 30 min at 4°C as follows: CD4–phycoerythrin (PE) (eBioscience, 25-0042-81, 1:400), CD4–fluorescein isothiocyanate (FITC) (eBioscience, 11-0042-82, 1:400), CD195–peridin chlorophyll protein (PerCP)–efluor710 (eBioscience, 46-1951-80, 1:400), CD45-FITC (eBioscience, 11-0451-82, 1:400), CD45–Alexa Fluor 700 (eBioscience, 56-0451-82, 1:400), CD8a–allophycocyanin (APC) (eBioscience, 47-0081-82, 1:400), CD11b-PE (eBioscience, 12-0112-82, 1:400), Ly6G-FITC (Cell Signaling Technology, 88876S, 1:400), Ly6C-PE (eBioscience, 25-5932-80, 1:400), NK1.1-PE (eBioscience, 12-5941-82, 1:400), F4/80-eF450 (eBioscience, 48-4801-82, 1:400), CD45.1-APC-eF780 (eBioscience, 47-0453-82, 1:400), and CD45.2–APC (eBioscience, 17-0454-82, 1:400), and incubated for 30 min at 4°C. Cells were washed again and resuspended in PBS for flow cytometry measurement by flow cytometry using a Citole S (Beckman Coulter) and analyzed using FlowJo (BD Biosciences).

Single-cell RNA sequencing

Transportation of 3 ml of peripheral blood was collected in EDTA anticoagulation tubes to library. All the blood was centrifuged for 10 min at 400*g*. Supernatant was removed. The pellet was resuspended in ACK buffer (Miltenyi Biotec) to lyse red blood cell. After washing PBS containing 0.04% bovine serum albumin (BSA Sigma), the pellet was resuspended in a volume of sample buffer. Then, cell buffer was stained with AM and DRAQ7 dye to viability and cells were counted using a BD scanner.

The BD Rhapsody system was used to capture the transcriptomic information of the peripheral blood single cells. Single-cell capture was achieved by random distribution of a single-cell suspension across >200,000 microwells through a limited dilution approach. Beads with oligonucleotide barcodes were added to saturation so that a bead was paired with a cell in a microwell. The cells were lysed in the microwell to hybridize mRNA molecules to barcoded capture oligos on the beads. Beads were collected into a single tube for reverse transcription and Exo I digestion. Upon cDNA synthesis, each cDNA molecule was tagged on the 5′ end (that is, the 3′ end of a mRNA transcript) with a unique molecular identifier (UMI) and cell barcode indicating its cell of origin. Whole-transcriptome libraries were prepared using the BD Rhapsody single-cell whole-transcriptome amplification (WTA) workflow including random priming and extension (RPE), RPE amplification PCR, and WTA index PCR. The libraries were quantified using a High Sensitivity DNA chip (Agilent) on a Bioanalyzer 2200 and the Qubit High Sensitivity DNA assay (Thermo Fisher Scientific). Sequencing was performed by an Illumina sequencer (Illumina, San Diego, CA) on a 150–base pair paired-end run. All steps are completed by NovelBio.

scRNA-seq data analysis was performed by NovelBio Bio-Pharm Technology Co. Ltd. with NovelBrain Cloud Analysis Platform. We applied fastp with default parameter filtering the adaptor sequence and removed the low-quality reads to achieve the clean data. UMI-tools were applied for Single Cell Transcriptome Analysis to identify the cell barcode whitelist. The UMI-based clean data were mapped to human genome (Ensemble version 100) using STAR mapping with customized parameter from UMI-tools standard pipeline to obtain the UMI counts of each sample. Cells contained over 200 expressed genes, mitochondria UMI rate below 20% passed the cell quality filtering, and mitochondria genes were removed in the expression table. Seurat package (version: 3.1.4, https://satijalab.org/seurat/) was used for cell normalization and regression based on the

expression table according to the UMI counts of each sample and percent of mitochondria rate to obtain the scaled data. Since samples were processed and sequenced in batches, we used mutual nearest neighbor to remove potential batch effect. Subsequently, top 10 principals were used for tSNE construction and UMAP construction. Using graph-based cluster method (resolution = 0.8), we acquired the unsupervised cell cluster result based on the top 10 principals and we calculated the marker genes by FindAllMarkers function with Wilcoxon rank sum test algorithm and differential expression gene (DEG) analysis under the following criteria: (i) ln (fold change) > 0.25; (ii) adjusted P value < 0.05; (iii) minimal percentage > 0.1. To identify the cell type detailed, the clusters of the same cell type were selected for re-tSNE analysis, graph-based clustering, and marker analysis.

Neutrophil SMART-seq

Total mRNA was extracted from neutrophils in the brain, isolated by flow cytometry. RNA libraries were sequenced on the Illumina sequencing platform by LC-BIO Co. Ltd. (HangZhou, China). Differentially expressed genes were defined as fold change cutoff with $|\log_2 \text{ratio}| \geq 1$ and $P < 0.05$.

Electrophysiology

Slice electrophysiology was performed as previously described (*51*). Coronal sections (250 μm) containing the hippocampus were prepared in an ice-cold cutting solution containing 40 mM NaCl, 148.5 mM sucrose, 4 mM KCl, 1.25 mM NaH_2PO_4, 25 mM $NaHCO_3$, 0.5 mM $CaCl_2$, 7 mM $MgCl_2$, 10 mM glucose, 1 mM sodium ascorbate, 3 mM sodium pyruvate, and 3 mM myoinositol, saturated with 95% O_2 and 5% CO_2. Slices were then incubated in a 1:1 mixture of cutting solution and external solution at 32°C for 45 min. The external solution contained the following: 125 mM NaCl, 4.5 mM KCl, 2.5 mM $CaCl_2$, 1.3 mM $MgCl_2$, 1.25 mM NaH_2PO_4, 25 mM $NaHCO_3$, 15 mM sucrose, and 15 mM glucose, saturated with 95% O_2 and 5% CO_2. Slices were perfused with the external solution at a flow rate of 3 to 4 ml/min at 32°C. The hippocampal pyramidal neurons were identified and patched. The data were recorded using an IPA-2 integrated patch amplifier controlled with SutterPatch software (Sutter Instrument, Novato, CA, USA). In whole-cell current recording, intrinsic excitability was measured and evoked action potentials were elicited by 300-ms step current injections at 20-pA increments from −20 to +170 pA. The intracellular solution contains a K^+-based solution: 123 mM potassium gluconate, 10 mM Hepes, 0.2 mM EGTA, 8 mM NaCl, 2 mM Mg–adenosine triphosphate, 0.3 mM Na–guanosine triphosphate (pH 7.3), with an osmolarity of 270 to 280 mOsm. For mEPSC, the cells were held in voltage-clamp mode at −70 mV for 1 min after entering whole-cell patch-clamp recording mode to allow dialysis of the Cs^+ internal solution for a relatively complete block of the potassium channels. The amplitude and frequency of the mEPSCs were analyzed using SutterPatch software (Sutter Igor Pro). mEPSCs were recorded in the presence of bicuculline (10 μM) and tetrodotoxin (10 μM).

Golgi staining

Brain samples were kept in Golgi-Cox solution at room temperature in the dark overnight, then replaced with Golgi-Cox solution, and remained for 13 days in the same environment. After being washed with double-distilled water, the brain samples were transferred into tissue-protectant solution for 3 days at room temperature. Finally, 200-mm coronal sections were cut on a vibrating microtome (VT1200s, Leica, Germany) in protectant solution and distilled water, then transferred into 3:1 ammonia solution and distilled water twice, and subsequently into 5% sodium thiosulfate for 10 min in the dark, and transferred into distilled water twice again. All the slices were mounted on slides with 80% glycerol. All sections were imaged using a 100× oil objective on a Zeiss Axioskop2 Plus microscope (Carl Zeiss, Thornwood, NY) with AxioVision Rel.4.7 software. In detail, around 30 dendrites from three mice in each group were analyzed using the plugin NeuronJ 1.4.3 in ImageJ software (Fiji edition, National Institutes of Health). Thereafter, a plugin Cell Counter was used to calculate the number of spines on these dendrites.

Immunohistochemistry and fluorometric quantification of Evans blue

Evans blue (EB) dye (2% w/v in sterile saline) was intravenously administered via the tail vein at a dose of 4 ml/kg body weight. After a 2-hour circulation period to allow EB-albumin complex formation, mice were transcardially perfused with ice-cold PBS (pH 7.4) to remove intravascular dye. Brains were harvested, fixed in 4% paraformaldehyde for 24 hours at 4°C, and cryoprotected in 30% sucrose. Coronal sections (20 μm thickness) were mounted on glass slides and air-dried. Focal blue-stained regions indicative of BBB disruption were qualitatively analyzed and photographed.

For fluorometric quantification of EB, brain tissues were homogenized in 1 ml of formamide per 100 mg of tissue using a glass homogenizer. Homogenates were incubated at 60°C for 24 hours to extract EB and centrifuged at 12,000*g* for 15 min, and supernatants were collected. Fluorescence intensity was measured using Varioskan Flash3001 at excitation/emission wavelengths of 620/680 nm. A standard curve was generated with serial dilutions of EB in formamide (1 to 50 ng/ml) for quantification. EB content was expressed as nanograms per milligram of brain tissue (ng/mg). All procedures were performed under dim light to minimize photobleaching.

Bone marrow chimeras

The recipient mice were subjected to lethal-dose irradiation (10 Gy), and 24 hours later, bone marrow cells (1×10^7) from the donor mice were intravenously injected into lethally irradiated mice. Under these conditions, the radio-resistant CNS-resident cells can be retained; however, bone marrow and peripheral blood cells would be replaced by bone marrow cells from donor mice. After 8 weeks, the chimeric mice can be subjected to CSDS procedure.

Electron microscopy

Mice were perfused with 2.5% glutaraldehyde and 2% paraformaldehyde in phosphate buffer (0.1 M, pH 7.4). Brains were removed, and 1-mm coronal slices were cut at the hippocampus. Following the fixation, the tissue was processed through 2% osmium tetroxide and 4% uranyl acetate and then dehydrated in grades of alcohol. The samples were placed in propyleneoxide for 1 hour and subsequently infiltrated overnight in a 1:1 mixture of propyleneoxide and EPON resin. The following day, the samples were embedded and polymerized at 60°C for 48 hours. Ultrathin sections (about 60 nm) were cut on an ultramicrotome, placed onto copper grids, stained with uranyl acetate and lead citrate, and examined on a Philips CM10 transmission electron microscope.

RNAscope in situ hybridization

Fluorescence in situ hybridization (FISH) was done using the RNAscope Fluorescent Multiplex Kit V2 (323100, Advanced Cell Diagnostics Inc.). In situ hybridization protocol was performed following recommended specifications for murine brain tissue. Probes against murine *Ccl5* and *Ly6g* were commercially available from Advanced Cell Diagnostics Inc. FISH protocol on murine brains was followed by fluorescence immunostaining according to the manufacturer's protocol.

Quantitative reverse transcription PCR

As previously described (*52*), total RNA was extracted from hippocampus tissues with TRIzol reagent (Invitrogen, USA). Reverse transcription PCR was carried out using a TAKARA PrimeScript RT reagent kit, and qPCR was performed in duplicate for each sample using a QuantiTect SYBR Green PCR kit (Qiagen, Germany) with an ABI 7300 Fast Real-Time PCR System (Applied Biosystems, Foster City, CA, USA). *Gapdh* was used as an internal control for the real-time PCR amplification. The sequences of primers used are as follows: *Ccl2*, CTGTGCTGACCCCAAGAAGG (forward) and TTGAGGTGGTTGTGGAAAAGG (reverse); *Ccl3*, TTCTCTGTACCATGACACTCTGC (forward) and CGTGGAATCTTCCGGCTGTAG (reverse); *Ccl4*, TTCCTGCTGTTTCTCTTACACC (forward) and CTGTCTGCCTCTTTTGGTCAG (reverse); *Ccl5*, GACACCACTCCCTGCTGCTT (forward) and ACACTTGGCGGTTCCTTCG (reverse); *Ccl7*, TGGGAAGCTGTTATCTTCAAGACA (forward) and CTCGACCCACTTCTGATGGG (reverse); *Ccl8*, GCGAGTGCTTCTTTGCCTG (forward) and TCTGGCCCAGTCAGCTTCTC (reverse); *Ccl11*, CATGACCAGTAAGAAGATCCC (forward) and CTTGAAGACTATGGCTTTCAGG (reverse); *Ccl12*, GCTGGACCAGATGCGGTG (forward) and CCGGACGTGAATCTTCTGCT (reverse); *Ccl20*, GCCTCTCGTACATACAGACGC (forward) and CCAGTTCTGCTTTGGATCAGC (reverse); *Ccl24*, CGGCCTCCTTCTCCTGGTA (forward) and TGGCCAACTGGTAGCTAACCA (reverse); *Ccl25*, GTTTTGTTGGGGCCTGGATG (forward) and ACTCCTCACGCTTGTACTGTTG (reverse); *Ccl26*, TCTTCGATTTGGGTCTCCTTG (forward) and CAGCTCCATGGGATCACATAG (reverse); *Cxcl1*, ACCGAAGTCATAGCCACACTC (forward) and CTCCGTTACTTGGGGACACC (reverse); *Cxcl2*, GGCCACCAACCACCAGGCTA (forward) and TTCCGTTGAGGGACAGCAGCC (reverse); *Cxcl8*, ATGACTTCCAAGCTGGCCGTGG (forward) and CATAATTTCTGTTTGGCGCAGTGTGG (reverse); *Cxcl9*, GCTCTGCCATGAAGTCCGCTGT (forward) and GCAATTGGGGCTTGGGGCAA (reverse); *Cxcl10*, AGCGCTTCATCCACCGCTGA (forward) and GGGCAGGATAGGCTCGCAGG (reverse); *Cxcl11*, CCCGAGTAACGGCTGCGACA (forward) and GGGCTCACAGTCAGACGTTCCC (reverse); *Cxcl12*, GCCCTTCAGATTGTAGCCCGGCT (forward) and TCCACTTTAGCTTCGGGTC AATGCA (reverse); *Gapdh*, CAAAAGGGTCATCTCC (forward) and CCCCAGCATCAAAGGTG (reverse).

WB analysis

Brain tissues were homogenized in radioimmunoprecipitation assay (RIPA) lysis buffer. The protein was separated and transferred onto polyvinylidene difluoride (PVDF) membranes (IPVH00010, Millipore, Billerica, MA, USA). Membranes were incubated with the following primary antibodies overnight at 4°C. Immuno-reactive bands were detected by ImageQuant LAS 4000 imaging system (GE Healthcare, Pittsburgh, PA, USA) and quantified using ImageJ software. The following primary antibodies were used: anti-Ly6G (ab25377, 1:400, Abcam), anti-CCR5 (ab7346, 1:500, Abcam), anti-CCL5 (AF478, 1:500, R&D Systems, USA), anti-PSD95 (20665-1-AP, 1:10,000, Proteintech), anti-SYP (17785-1-AP, 1:10,000, Proteintech), and anti–β-actin (BM0627, Boster, Pleasanton, CA, USA). Full-length WBs are available in fig. S15.

Statistical analysis

All data were analyzed using Prism9 software. All results were shown as means ± SEM. One-way or two-way analysis of variance (ANOVA) with the Tukey's post hoc test was used for comparison among different treatments and genotypes, and Student's *t* test was used to assess the differences between two groups. The results were considered significant at $P < 0.05$.

Supplementary Materials

This PDF file includes:

Figs. S1 to S15

REFERENCES AND NOTES

1. Z. Fan, J. Chang, Y. Liang, H. Zhu, C. Zhang, D. Zheng, J. Wang, Y. Xu, Q. J. Li, H. Hu, Neural mechanism underlying depressive-like state associated with social status loss. *Cell* **186**, 560–576.e17 (2023).
2. S. Marwaha, E. Palmer, T. Suppes, E. Cons, A. H. Young, R. Upthegrove, Novel and emerging treatments for major depression. *Lancet* **401**, 141–153 (2023).
3. R. S. Duman, G. K. Aghajanian, Synaptic dysfunction in depression: Potential therapeutic targets. *Science* **338**, 68–72 (2012).
4. E. Sarno, A. J. Moeser, A. J. Robison, Neuroimmunology of depression. *Adv. Pharmacol.* **91**, 259–292 (2021).
5. B. M. Balog, A. Sonti, R. E. Zigmond, Neutrophil biology in injuries and diseases of the central and peripheral nervous systems. *Prog. Neurobiol.* **228**, 102488 (2023).
6. N. Dhanesha, R. B. Patel, P. Doddapattar, M. Ghatge, G. D. Flora, M. Jain, D. Thedens, H. Olalde, M. Kumskova, E. C. Leira, A. K. Chauhan, PKM2 promotes neutrophil activation and cerebral thromboinflammation: Therapeutic implications for ischemic stroke. *Blood* **139**, 1234–1245 (2022).
7. E. Zenaro, E. Pietronigro, V. Della Bianca, G. Piacentino, L. Marongiu, S. Budui, E. Turano, B. Rossi, S. Angiari, S. Dusi, A. Montresor, T. Carlucci, S. Nani, G. Tosadori, L. Calciano, D. Catalucci, G. Berton, B. Bonetti, G. Constantin, Neutrophils promote Alzheimer's disease-like pathology and cognitive decline via LFA-1 integrin. *Nat. Med.* **21**, 880–886 (2015).
8. R. A. Drummond, M. Swamydas, V. Oikonomou, B. Zhai, I. M. Dambuza, B. C. Schaefer, A. C. Bohrer, K. D. Mayer-Barber, S. A. Lira, Y. Iwakura, S. G. Filler, G. D. Brown, B. Hube, J. R. Naglik, T. M. Hohl, M. S. Lionakis, CARD9^{+} microglia promote antifungal immunity via IL-1β- and CXCL1-mediated neutrophil recruitment. *Nat. Immunol.* **20**, 559–570 (2019).
9. G. Shi, L. Liu, Y. Cao, G. Ma, Y. Zhu, J. Xu, X. Zhang, T. Li, L. Mi, H. Jia, Y. Zhang, X. Liu, Y. Zhou, S. Li, G. Yang, X. Liu, F. Chen, B. Wang, Q. Deng, S. Zhang, J. Zhang, Inhibition of neutrophil extracellular trap formation ameliorates neuroinflammation and neuronal apoptosis via STING-dependent IRE1α/ASK1/JNK signaling pathway in mice with traumatic brain injury. *J. Neuroinflammation* **20**, 222 (2023).
10. E. Beurel, M. Toups, C. B. Nemeroff, The bidirectional relationship of depression and inflammation: Double trouble. *Neuron* **107**, 234–256 (2020).
11. P. Cao, C. Chen, A. Liu, Q. Shan, X. Zhu, C. Jia, X. Peng, M. Zhang, Z. Farzinpour, W. Zhou, H. Wang, J. N. Zhou, X. Song, L. Wang, W. Tao, C. Zheng, Y. Zhang, Y. Q. Ding, Y. Jin, L. Xu, Z. Zhang, Early-life inflammation promotes depressive symptoms in adolescence via microglial engulfment of dendritic spines. *Neuron* **109**, 2573–2589.e9 (2021).
12. G. E. Hodes, M. L. Pfau, M. Leboeuf, S. A. Golden, D. J. Christoffel, D. Bregman, N. Rebusi, M. Heshmati, H. Aleyasin, B. L. Warren, B. Lebonte, S. Horn, K. A. Lapidus, V. Stelzhammer, E. H. Wong, S. Bahn, V. Krishnan, C. A. Bolanos-Guzman, J. W. Murrough, M. Merad, S. J. Russo, Individual differences in the peripheral immune system promote resilience versus susceptibility to social stress. *Proc. Natl. Acad. Sci. U.S.A.* **111**, 16136–16141 (2014).
13. G. E. Hodes, V. Kana, C. Menard, M. Merad, S. J. Russo, Neuroimmune mechanisms of depression. *Nat. Neurosci.* **18**, 1386–1393 (2015).
14. S. Harsanyi, I. Kupcova, L. Danisovic, M. Klein, Selected biomarkers of depression: What are the effects of cytokines and inflammation? *Int. J. Mol. Sci.* **24**, 578 (2023).
15. K. Shi, H. Li, T. Chang, W. He, Y. Kong, C. Qi, R. Li, H. Huang, Z. Zhu, P. Zheng, Z. Ruan, J. Zhou, F. D. Shi, Q. Liu, Bone marrow hematopoiesis drives multiple sclerosis progression. *Cell* **185**, 2234–2247.e17 (2022).
16. Z. Shi, P. Yu, W. J. Lin, S. Chen, X. Hu, S. Chen, J. Cheng, Q. Liu, Y. Yang, S. Li, Z. Zhang, J. Xie, J. Jiang, B. He, Y. Li, H. Li, Y. Xu, J. Zeng, J. Huang, J. Mei, J. Cai, J. Chen, L. J. Wu, H. Ko,

Y. Tang, Microglia drive transient insult-induced brain injury by chemotactic recruitment of CD8$^+$ T lymphocytes. *Neuron* **111**, 696–710.e9 (2023).
17. B. D. Michael, L. Bricio-Moreno, E. W. Sorensen, Y. Miyabe, J. Lian, T. Solomon, E. A. Kurt-Jones, A. D. Luster, Astrocyte- and neuron-derived CXCL1 drives neutrophil transmigration and blood-brain barrier permeability in viral encephalitis. *Cell Rep.* **32**, 108150 (2020).
18. Y. M. Khaw, A. Tierney, C. Cunningham, K. Soto-Diaz, E. Kang, A. J. Steelman, M. Inoue, Astrocytes lure CXCR2-expressing CD4$^+$ T cells to gray matter via TAK1-mediated chemokine production in a mouse model of multiple sclerosis. *Proc. Natl. Acad. Sci. U.S.A.* **118**, e2017213118 (2021).
19. M. Amitai, S. Kaffman, E. Kroizer, M. Lebow, I. Magen, N. Benaroya-Milshtein, S. Fennig, A. Weizman, A. Apter, A. Chen, Neutrophil to-lymphocyte and platelet-to-lymphocyte ratios as biomarkers for suicidal behavior in children and adolescents with depression or anxiety treated with selective serotonin reuptake inhibitors. *Brain Behav. Immun.* **104**, 31–38 (2022).
20. G. Ozyurt, N. C. Binici, Increased neutrophil-lymphocyte ratios in depressive adolescents is correlated with the severity of depression. *Psychiatry Res.* **268**, 426–431 (2018).
21. F. Cathomas, H. Y. Lin, K. L. Chan, L. Li, L. F. Parise, J. Alvarez, R. Durand-de Cuttoli, A. V. Aubry, S. Muhareb, F. Desland, Y. Shimo, A. Ramakrishnan, M. Estill, C. Ferrer-Perez, E. M. Parise, C. M. Wilk, M. P. Kaster, J. Wang, A. Sowa, W. G. Janssen, S. Costi, A. Rahman, N. Fernandez, M. Campbell, F. K. Swirski, E. J. Nestler, L. Shen, M. Merad, J. W. Murrough, S. J. Russo, Circulating myeloid-derived MMP8 in stress susceptibility and depression. *Nature* **626**, 1108–1115 (2024).
22. C. Menard, M. L. Pfau, G. E. Hodes, V. Kana, V. X. Wang, S. Bouchard, A. Takahashi, M. E. Flanigan, H. Aleyasin, K. B. LeClair, W. G. Janssen, B. Labonte, E. M. Parise, Z. S. Lorsch, S. A. Golden, M. Heshmati, C. Tamminga, G. Turecki, M. Campbell, Z. A. Fayad, C. Y. Tang, M. Merad, S. J. Russo, Social stress induces neurovascular pathology promoting depression. *Nat. Neurosci.* **20**, 1752–1760 (2017).
23. M. A. Giese, L. E. Hind, A. Huttenlocher, Neutrophil plasticity in the tumor microenvironment. *Blood* **133**, 2159–2167 (2019).
24. Y. Cho, G. Szabo, Two faces of neutrophils in liver disease development and progression. *Hepatology* **74**, 503–512 (2021).
25. P. X. Liew, P. Kubes, The neutrophil's role during health and disease. *Physiol. Rev.* **99**, 1223–1248 (2019).
26. Q. Mu, K. Yao, M. Z. Syeda, M. Zhang, Q. Cheng, Y. Zhang, R. Sun, Y. Lu, H. Zhang, Z. Luo, H. Huang, X. Liu, C. Luo, X. Zhu, S. Wu, L. Cui, C. Huang, X. Chen, L. Tang, Ligustrazine nanoparticle hitchhiking on neutrophils for enhanced therapy of cerebral ischemia-reperfusion injury. *Adv. Sci.* **10**, e2301348 (2023).
27. L. C. D. Smyth, H. C. Murray, M. Hill, E. van Leeuwen, B. Highet, N. J. Magon, M. Osanlouy, S. N. Mathiesen, B. Mockett, M. K. Singh-Bains, V. K. Morris, A. N. Clarkson, M. A. Curtis, W. C. Abraham, S. M. Hughes, R. L. M. Faull, A. J. Kettle, M. Dragunow, M. B. Hampton, Neutrophil-vascular interactions drive myeloperoxidase accumulation in the brain in Alzheimer's disease. *Acta Neuropathol. Commun.* **10**, 38 (2022).
28. W. C. Poller, J. Downey, A. A. Mooslechner, N. Khan, L. Li, C. T. Chan, C. S. McAlpine, C. Xu, F. Kahles, S. He, H. Janssen, J. E. Mindur, S. Singh, M. G. Kiss, L. Alonso-Herranz, Y. Iwamoto, R. H. Kohler, L. P. Wong, K. Chetal, S. J. Russo, R. I. Sadreyev, R. Weissleder, M. Nahrendorf, P. S. Frenette, M. Divangahi, F. K. Swirski, Brain motor and fear circuits regulate leukocytes during acute stress. *Nature* **607**, 578–584 (2022).
29. X. Zhang, B. Lei, Y. Yuan, L. Zhang, L. Hu, S. Jin, B. Kang, X. Liao, W. Sun, F. Xu, Y. Zhong, J. Hu, H. Qi, Brain control of humoral immune responses amenable to behavioural modulation. *Nature* **581**, 204–208 (2020).
30. R. Mou, J. Ma, X. Ju, Y. Wu, Q. Chen, J. Li, T. Shang, S. Chen, Y. Yang, Y. Li, K. Lv, X. Chen, Q. Zhang, T. Liang, Y. Feng, X. Lu, Vasopressin drives aberrant myeloid differentiation of hematopoietic stem cells, contributing to depression in mice. *Cell Stem Cell* **31**, 1794–1812.e10 (2024).
31. F. Denorme, I. Portier, J. L. Rustad, M. J. Cody, C. V. de Araujo, C. Hoki, M. D. Alexander, R. Grandhi, M. R. Dyer, M. D. Neal, J. J. Majersik, C. C. Yost, R. A. Campbell, Neutrophil extracellular traps regulate ischemic stroke brain injury. *J. Clin. Invest.* **132**, e154225 (2022).
32. K. Vaibhav, M. Braun, K. Alverson, H. Khodadadi, A. Kutiyanawalla, A. Ward, C. Banerjee, T. Sparks, A. Malik, M. H. Rashid, M. B. Khan, M. F. Waters, D. C. Hess, A. S. Arbab, J. R. Vender, N. Hoda, B. Baban, K. M. Dhandapani, Neutrophil extracellular traps exacerbate neurological deficits after traumatic brain injury. *Sci. Adv.* **6**, eaax8847 (2020).
33. J. Jin, F. Wang, J. Tian, X. Zhao, J. Dong, N. Wang, Z. Liu, H. Zhao, W. Li, G. Mang, S. Hu, Neutrophil extracellular traps contribute to coagulopathy after traumatic brain injury. *JCI Insight* **8**, e141110 (2023).
34. X. J. Xu, Q. Q. Ge, M. S. Yang, Y. Zhuang, B. Zhang, J. Q. Dong, F. Niu, H. Li, B. Y. Liu, Neutrophil-derived interleukin-17A participates in neuroinflammation induced by traumatic brain injury. *Neural Regen. Res.* **18**, 1046–1051 (2023).
35. S. E. Holmes, D. Scheinost, S. J. Finnema, M. Naganawa, M. T. Davis, N. DellaGioia, N. Nabulsi, D. Matuskey, G. A. Angarita, R. H. Pietrzak, R. S. Duman, G. Sanacora, J. H. Krystal, R. E. Carson, I. Esterlis, Lower synaptic density is associated with depression severity and network alterations. *Nat. Commun.* **10**, 1529 (2019).
36. L. Speranza, Y. Inglebert, C. De Sanctis, P. Y. Wu, M. Kalinowska, R. A. McKinney, A. Francesconi, Stabilization of Spine Synaptopodin by mGluR1 Is Required for mGluR-LTD. *J. Neurosci.* **42**, 1666–1678 (2022).
37. Q. Gong, W. Li, T. Ali, Y. Hu, S. Mou, Z. Liu, C. Zheng, R. Gao, A. Li, T. Li, N. Li, Z. Yu, S. Li, eIF4E phosphorylation mediated LPS induced depressive-like behaviors via ameliorated neuroinflammation and dendritic loss. *Transl. Psychiatry* **13**, 352 (2023).
38. E. S. Wohleb, R. Terwilliger, C. H. Duman, R. S. Duman, Stress-induced neuronal colony stimulating factor 1 provokes microglia-mediated neuronal remodeling and depressive-like behavior. *Biol. Psychiatry* **83**, 38–49 (2018).
39. Y. M. Khaw, C. Cunningham, A. Tierney, M. Sivaguru, M. Inoue, Neutrophil-selective deletion of Cxcr2 protects against CNS neurodegeneration in a mouse model of multiple sclerosis. *J. Neuroinflammation* **17**, 49 (2020).
40. X. Chen, M. Firulyova, M. Manis, J. Herz, I. Smirnov, E. Aladyeva, C. Wang, X. Bao, M. B. Finn, H. Hu, I. Shchukina, M. W. Kim, C. M. Yuede, J. Kipnis, M. N. Artyomov, J. D. Ulrich, D. M. Holtzman, Microglia-mediated T cell infiltration drives neurodegeneration in tauopathy. *Nature* **615**, 668–677 (2023).
41. M. Jorfi, J. Park, C. K. Hall, C. J. Lin, M. Chen, D. von Maydell, J. M. Kruskop, B. Kang, Y. Choi, D. Prokopenko, D. Irimia, D. Y. Kim, R. E. Tanzi, Infiltrating CD8$^+$ T cells exacerbate Alzheimer's disease pathology in a 3D human neuroimmune axis model. *Nat. Neurosci.* **26**, 1489–1504 (2023).
42. D. D. Shi, Y. D. Zhang, S. Zhang, B. B. Liao, M. Y. Chu, S. Su, K. Zhuo, H. Hu, C. Zhang, Z. Wang, Stress-induced red nucleus attenuation induces anxiety-like behavior and lymph node CCL5 secretion. *Nat. Commun.* **14**, 6923 (2023).
43. S. P. Leighton, L. Nerurkar, R. Krishnadas, C. Johnman, G. J. Graham, J. Cavanagh, Chemokines in depression in health and in inflammatory illness: A systematic review and meta-analysis. *Mol. Psychiatry* **23**, 48–58 (2018).
44. E. Beurel, J. A. Lowell, R. S. Jope, Distinct characteristics of hippocampal pathogenic T_H17 cells in a mouse model of depression. *Brain Behav. Immun.* **73**, 180–191 (2018).
45. E. Beurel, L. E. Harrington, R. S. Jope, Inflammatory T helper 17 cells promote depression-like behavior in mice. *Biol. Psychiatry* **73**, 622–630 (2013).
46. F. Li, S. Y. Jiang, T. Tian, W. J. Li, Y. Xue, R. H. Du, G. Hu, M. Lu, Kir6.1/K-ATP channel in astrocytes is an essential negative modulator of astrocytic pyroptosis in mouse model of depression. *Theranostics* **12**, 6611–6625 (2022).
47. S. Y. Jiang, T. Tian, H. Yao, X. M. Xia, C. Wang, L. Cao, G. Hu, R. H. Du, M. Lu, The cGAS-STING-YY1 axis accelerates progression of neurodegeneration in a mouse model of Parkinson's disease via LCN2-dependent astrocyte senescence. *Cell Death Differ.* **30**, 2280–2292 (2023).
48. S. Y. Jiang, T. Tian, W. J. Li, T. Liu, C. Wang, G. Hu, R. H. Du, Y. Liu, M. Lu, Mefloquine targets NLRP3 to reduce lipopolysaccharide-induced systemic inflammation and neural injury. *EMBO Rep.* **24**, e57101 (2023).
49. B. Wang, Y. Ma, S. Li, H. Yao, M. Gu, Y. Liu, Y. Xue, J. Ding, C. Ma, S. Yang, G. Hu, GSDMD in peripheral myeloid cells regulates microglial immune training and neuroinflammation in Parkinson's disease. *Acta Pharm. Sin. B* **13**, 2663–2679 (2023).
50. Z. Li, J. Li, Y. Wei, W. Zou, O. E. Vidjro, J. Wang, L. Zhou, Y. Zhu, T. Ma, aBLA and pBLA projections of cell type-specific D1 neurons from the mPFC differentially control alcohol-seeking behavior. *Biol. Psychiatry* **95**, 963–973 (2024).
51. Z. Li, O. E. Vidjro, G. Guo, Y. Du, Y. Zhou, Q. Xie, J. Li, K. Gao, L. Zhou, T. Ma, NLRP3 deficiency decreases alcohol intake controlling anxiety-like behavior via modification of glutamatergic transmission in corticostriatal circuits. *J. Neuroinflammation* **19**, 308 (2022).
52. M. M. Chen, Z. L. Hu, J. H. Ding, R. H. Du, G. Hu, Astrocytic Kir6.1 deletion aggravates neurodegeneration in the lipopolysaccharide-induced mouse model of Parkinson's disease via astrocyte-neuron cross talk through complement C3-C3R signaling. *Brain Behav. Immun.* **95**, 310–320 (2021).

Acknowledgments: We thank Y. Shuo (Nanjing Medical University) for donating CD45.1 mice. **Funding:** This work was supported by grants from the National Key R&D Program of China (no. 2021ZD0202903 to M.L.) and the National Natural Science Foundation of China (nos. 82373851 and 82173797 to M.L. and 82273906 to R.-H.D.). **Author contributions:** Conceptualization: M.L., R.-H.D., G.H., H.Y., and S.-Y.J. Data curation: H.Y., S.-Y.J., Y.-Y.J., Z.-Y.Z., Z.Z., and M.L. Formal analysis: H.Y., S.-Y.J., Y.-Y.J., Z.-Y.Z., Z.Z., and M.L. Funding acquisition: M.L. and R.-H.D. Investigation: H.Y., Y.-Y.J., T.-F.M., Z.Z., M.L., and C.W. Methodology: H.Y., S.-Y.J., Y.-Y.J., Z.-Y.Z., Z.Z., T.-F.M., M.L., and C.W. Project administration: M.L. and R.-H.D. Resources: S.-Y.J., Y.-Y.J., Z.Z., K.-Z.Z., and M.L. Software: S.-Y.J. Supervision: M.L. and R.-H.D. Validation: H.Y., S.-Y.J., Y.-Y.J., Z.-Y.Z., Z.Z., and M.L. Visualization: Z.Z., S.-Y.J., M.L., and R.-H.D. Writing—original draft: H.Y. and R.-H.D. Writing—review and editing: S.-Y.J., G.H., M.L., and R.-H.D. **Competing interests:** The authors declare that they have no competing interests. **Data and materials availability:** All data needed to evaluate the conclusions in the paper are present in the paper and/or the Supplementary Materials.

Submitted 6 October 2024
Accepted 17 April 2025
Published 21 May 2025
10.1126/sciadv.adt6632